The Depositional and Clast Provenance Age of the Coodnambana Metaconglomerate, Mount Woods Inlier

Sean O'Sullivan

Supervisors: Caroline Forbes & David Giles

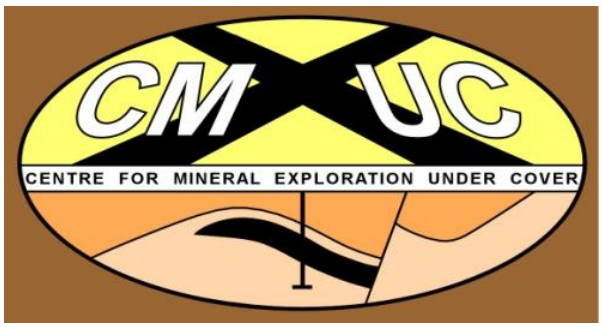

November 2010

Contents:

The Depositional and Clast Provenance Age of the Coodnambana Metaconglomerate, Mount Woods Inlier

ABSTRACT

Laser Ablation Inductively Coupled Plasma-Mass Spectrometry U-Pb zircon and monazite geochronology for the Coodnambana Metaconglomerate has been used to constrain detrital ages and the provenance of the interpreted youngest sequence in the Mount Woods Inlier. U-Pb zircon and monazite ages include data from the quartzite underlying the Coodnambana Metaconglomerate, the quartz-magnetite metapsammitic clast and conglomerate matrix. These ages are 1725, 1808 and 1558 Ma respectively. These data indicate that the clasts were not sourced from the Skylark Metasediments and does not directly imply the presence of an unconformity at the base of the Coodnambana Metaconglomerate. The provenance of these clasts is currently unknown. We propose an alternate single stage depositional and tectonothermal model for the Mount Woods Inlier, in which sedimentation occurred from ca. 1750 Ma to ca. 1630 Ma and possibly up to 1590 Ma. At ca. 1590 sedimentation ceased with the onset of metamorphism and deformation. Metamorphic conditions reach ~4.7kbar and 750^{o}C. Following metamorphism the Mount Woods Inlier experience a hydrothermal event at ca. 1558 Ma.

INTRODUCTION

Eastern Proterozoic Australia (Fig. 1) records a diverse range of magmatic, metamorphic, deformation and mineralisation events between 1.78 – 1.56 Ga. The tectonic regime of eastern Proterozoic Australia was an accretionary margin and a suggested north dipping (Giles *et al.* 2002) or south dipping (Wade *et al.* 2008) subduction zone along the southern margin of the North Australian Craton. Basins developed between 1.8 – 1.6 Ga within the overriding plate in a transpressional stress regime (Scott *et al.* 2000, Giles *et al.* 2002). Remnants of these basins include the McArthur basin (Rawlings 1999), Mount Isa Inlier (Page *et al.* 2000b), Georgetown Inlier (Withnall *et al.* 1988) and Curnamona Craton (Black *et al.* 1998, Betts *et al.* 2002). These basins all show

variably deformed low-pressure/high-temperature metamorphosed supracrustal and intrusive rocks (e.g. Black *et al.* 1998, Betts *et al.* 2002, Forbes *et al.* 2008). From 1.60 – 1.58 Ga eastern Proterozoic Australia experienced a period of interrupted basin development through orogenesis (Betts *et al.* 2002). Evidence of this orogenic event is found in Mt Isa (Isan Orogeny, ca. 1600 - 1500 Ma, Giles & Nutman 2002), Curnamona Craton (Olarian Orogeny, ca. 1.60-1.59Ga, Page *et al.* 2000a), and the northern Gawler Craton (Late Kararan Orogeny, ca. 1.58-1.54 Ga, Daly *et al.* 1998). The eastern margin of Proterozoic Australia is characterised by a tectonothermal event represented by the voluminous outpouring of bimodal volcanic rocks and the emplacement of the Hiltaba Granites (Gawler Craton, ca. 1600 - 1585 Ma, Daly *et al.* 1998), the Williams and Naraku Batholith (Mt Isa Inlier, ca. 1500 Ma, Wyborn 1998) and the Mt Neill Granite (Mt Painter Inlier, ca. 1575 Ma & ca. 1555 Ma, Elburg *et al.* 2001). Szpunar *et al.* (2007) has suggested that the Eastern Gawler Cration and the Broken Hill Block may share a similar tectonothermal history and are separated by the Adelaide Rift Complex; suggesting that these two terrains may have been proximal to each other during the Proterozoic.

In this paper I present evidence for the relative timing of deposition, metamorphism and deformation of the youngest stratigraphic unit currently recognised within the Mount Woods Inlier. This has been done by structural mapping and monazite and zircon U-Pb LA ICP-MS geochronology of selected units and is used to postulate alternative depositional and tectonothermal histories for the Mount Woods Inlier.

GEOLOGICAL SETTING OF THE MOUNT WOODS INLIER

The Mount Woods Inlier is within the northern Gawler Craton (Fig. 1) and is a structurally complex area that records multiple deformation events and upper amphibolite to granulite facies metamorphism (Flint & Benbow 1977, Betts *et al.* 2003, Chalmers 2007b). The sedimentary successions of the Mount Woods Inlier are interpreted to have been deposited onto the passive margin of an Archean continent during the Paleoproterozoic (Betts *et al.* 2003). Chalmers (2007b) divided the Mount Woods Complex into the Skylark Metasediments, the Coodnambana Metaconglomerate and intrusive igneous units that pre-date Hiltaba Suite equivalents. The Skylark Metasediments include the bulk of the metasedimentary units in the Mount Woods Complex and consist of metapelitic and metapsammitic lithologies (Chalmers 2007b). Chalmers (2007b) and Jagodzinski (2007)

dated two samples of the Skylark Metasediments from Moonlight Hill using the zircon U-Pb SHRIMP method in order to establish a definite date for peak metamorphism and to investigate complex populations of detrital zircons. The two analysed samples were the magnetic psammitic sediment and garnet-cordierite-spinel-sillimanite pelite (Jagodzinski *et al.* 2007b, Chalmers 2007b). The magnetic psammitic sediment yielded a unimodal age of 1752±6Ma with a minor population at ~1850 Ma and the garnet-cordierite-spinel-sillimanite pelite yielded a unimodal age of 1749±6Ma. Holm (OZCHRON) has reported younger maxiumum depositional ages from drill core within the Mount Woods Inlier. These ages include provenance clusters at 1670±13, 1627±19 and 1736±13 Ma from a felsic gneiss within drill hole Engenina 61 and 1750±6 and 1652±22 Ma from a quartzite within drill hole Engenina 38 (Fig. 2) (Holm, OZCHRON). Currently the exact relationship of these sediments to the Skylark Metasediments is unknown and Neumann & Fraser (2007) suggested that these ages may represent a second post-Kimban sedimentary package. Betts et al. (2003) interpreted that the Coodnambana Metaconglomerate unconformably overlies the Skylark Metasediments based on the observation that the clasts within the conglomerate were sourced from the Skylark Metasediments. This package has been interpreted as a second sedimentary sequence consisting of a quartzite, polymictic metaconglomerate and interbedded psammite (Betts *et al.* 2003). Chalmers (2007b) and Jagodzinski (2007) dated the interbedded psammite using the U-Pb SHRIMP technique, this unit yielded a unimodal detrital age of 1749±6Ma with a minor detrital component of ~1850 Ma and metamorphic rims yielding an age of 1595±10Ma. Various igneous intrusive units are found within the Mount Woods Inlier, including the igneous porphyblastic gneiss, orthogneiss, Engenina Adamellite (ca. 1692 Ma, Fanning 1997a, Daly *et al.* 1998) and Balta Granite (ca. 1584 Ma, Fanning 1997a, Daly *et al.* 1998) (Hiltaba Suite equivalent) (Benbow & Flint 1979, Betts *et al.* 2003, Chalmers 2007a, 2007b).

The earliest deformation event to affect the Mount Woods Inlier was the Kimban Orogeny (ca. 1.73-1.69 Ga, Hoek & Schaefer 1998, Vassallo & Wilson 2001, Betts *et al.* 2003). In the Mount Woods Inlier, the early stages of the Kimban Orogeny involved the development of tight to isoclinal folds with an axial planar gneissic to schistose fabric (Betts *et al.* 2003). These structures were overprinted by open to isoclinal folds with south to southeast trending axial traces (Betts *et al.* 2003). The variation in the orientation of the second generation structures has been attributed to the synchronous emplacement of the Engenina Adamellite (ca. 1692 Ma,

Fanning 1997a, Daly *et al.* 1998) which affected the local stress regime (Betts *et al.* 2003). Finlay (1993) and Betts *et al.* (2003) interpreted the Kimban Orogeny to be synchronous with peak metamorphism in the inlier at ca. 1736 Ma based on a U-Pb zircon age of a first generation partial melt at Spire Hills (Fig. 3). Following the emplacement of the Engenina Adamellite, discrete shear zones and localised folds developed throughout the inlier and the metamorphic rocks were exhumed during the Early Kararan Orogeny (Betts *et al.* 2003) ca 1.69 – 1.67 Ga (Daly *et al.* 1998). These sequences were eroded and unconformably overlain by interbedded sandstones and the Coodnambana Metaconglomerates (Betts *et al.* 2003).These sediments were later contact metamorphosed by shallow level intrusive of the Balta Granite Suite (Betts *et al.* 2003) ca. 1584 Ma (Daly *et al.* 1998). The Balta Granite Suite is suggested to be equivalent to the Hiltaba Granite Suite (Creaser & White 1991, Creaser & Cooper 1993, Daly *et al.* 1998). Conversely, Forbes *et al.* (in review) suggested that peak metamorphic conditions were reached at ca. 1590 Ma (Jagodzinski *et al.* 2007a, Chalmers 2007b).

The Skylark Metasediments comprise variably deformed psammites and pelites including interbedded biotite - garnet schist and coarse quartz - feldspar gneiss, garnet - corderite - spinel - sillimanite pelite, porphyroblastic sillimanite pelite, clast rich magnetic textured melt sediment, thinly bedded psammitic - garnet pelite and magnetic psammitic sediment (Ambrose & Flint 1981, Chalmers 2007b). In addition to the metasediments a porphyroblastic gneiss and orthogneiss have been identified (Chalmers 2007b).

The Coodnambana Metaconglomerate is a polymictic conglomerate with a diverse clast composition that includes banded psammites, fine grained granites and coarse grained pegmatic fragments (Flint & Benbow 1977, Ambrose & Flint 1981, Chalmers 2007b). The provenance of these clasts has been suggested to be from the eroded Skylark Metasediemts (Betts *et al.* 2003, Chalmers 2007b). Chalmers (2007) recognised that the detrital age of the Coodnambana Metaconglomerate is consistent with the detrital age of the underlying Skylark Metasediments and hence suggests that the Coodnambana Metaconglomerate was derived from eroding of the Skylark Metasediments and was later metamorphosed at 1595Ma.

THE SPIRE HILLS AREA

The Spire Hills area is located in the southern Mount Woods Inlier (Fig. 3). The area has undergone upper amphibolite to granulite facies metamorphism (Betts *et al.* 2003). The Coodnambana Metaconglomerate is exposed at the western extent of this area. This is the only exposure of the Coodnambana Metaconglomerate and it provides an opportunity to investigate a proportion of the stratigraphy in the Mount Woods Inlier.

Lithology

The Skylark Metasediments

In the Spire Hills mapping area the dominant lithology of the Skylark Metasediments is the migmatitic iron formation (Betts *et al.* 2003). Exposed adjacent to the Coodnambana Metaconglomerate is the magnetite-biotite-cordierite feldspar gneiss (Fig. 4a,b). This unit is medium- to coarse-grained (0.5-1 mm) gneiss and appears as small (up to 1m) exposures in the basement rocks. The unit is approximately 30% quartz, 20% feldspar, 20% magnetite, 20% biotite and 10% cordierite. Cordierite forms porphyoblasts amongst the mafic layering, and quartz and k-feldspar occur as felsic bands. Just to the west of the mapping area is the garnet-biotite-sillimanite gneiss. This unit consists of 20% quartz, 20% k-feldspar, 20% biotite, 15% magnetite, 15% garnet and 10% sillimanite. The unit is a medium- to coarse-grained (0.5-1mm) and shows segregations of material forming mafic and felsic components. Garnet is very coarse-grained (up to 15mm) and the foliation wraps around these porphyroblasts.

The Coodnambana Metaconglomerate

The Coodnambana Metaconglomerate overlies the Skylark Metasediments at Spire Hills. The basal unit to the Coodnambana Metaconglomerate is a medium- to coarse-grained (0.5-1mm) quartzite that consists of a single homogeneous massive layer with an apparent thickness of 25m thick and it is only seen as a small outcrop within Spire Hills (Fig. 3). The unit comprises of >97% quartz with minor magnetite andalusite and sillimanite (Figure 5a). In thin section the quartz grains are anhedral coarse-grained (0.5-1mm) displaying inequigranular – interlobate texture and based on the interlobate nature and pinning microstructures of the quartz grain boundaries it underwent grain boundary migration recrystallisation (Figure 5b). Quartz grains display undulosed extinction (Figure 5c). Within the quartz matrix are medium-grained (0.5mm) andalusite that are often

surrounded by sillimanite (Figure 5a). The sillimanite is coarse-grained (~0.5-1mm) and typically occurs as anhedral patches of fibrous sillimanite displaying low order birefringence (Figure 5d). The bulk of the magnetite is seen within the andalusite – sillimanite porphroblasts and lesser anhedral to subhedral fine-grained (~0.25mm) magnetite is typically at quartz grain boundaries (Figure 5a).

The basal quartzite is overlain by a polymictic conglomerate; the contact between these two units is covered by colluvium and not exposed. The conglomerate is comprised of rounded clasts of variable composition within a hematite and quartz bearing matrix; the conglomerate is termed the Coodnambana Metaconglomerate (Fig. 7). Clast distribution appears random and no preferred orientation is visible. Metasedimentary clasts range in size from 4 to 50mm and clasts comprise rounded fine-grained (0.25-0.5mm) quartzite casts , coarse-grained (1-3mm) quartzite clasts and fine grained (~0.5mm) hematite-quartz metapsammitic clasts, and within an alternating hematite rich (mafic) and hematite – fine grained quartz (felsic) matrix in which the alternating bands are visible in hand specimen (Fig. 4c, 8).

The rounded coarse-grained quartz clasts consists of >99% quartz with minor hematite (Figure 5e). These clasts are distinctively coarse-grained (1-3mm). The quartz is generally a subhedral shape with a serate – polygonal texture. Hematite content is minor and occurs as medium-grained (~0.5mm) subhedral shaped grains along some quartz grain boundaries.

The rounded fine-grained quartz clast consists of >98% quartz with minor hematite. These clasts are distinctively fine-grained (0.25-0.5mm). The quartz is a subhedral shape and displays a equigranular – polygonal texture. Hematite is minor and occurs as fine-grained (0.25mm) subhedral shaped grains along some quartz grain boundaries.

The metapsammitic clasts consist of distinctive hematite and quartz banding which includes a folded quartz hematite clast (15-25mm) (Figure 5f) and a banded quartz hematite clast (5-15mm) (Figure 6g). The folded quartz hematite clast consists of well defined bands (0.5-3mm thick) that are comprised quartz rich and hematite rich layers; the quartz rich layers are approximately 70% quartz and 30% hematite and hematite rich layers are approximately 80% hematite and 20% quartz. These bands possibly represent primary layering. Within the banding are small fold structures; it is unclear whether these structures are folds of the primary bedding or folds

of small quartz veins. Some folds are seen to crosscut the primary layering and occur as thicker coarse-grained (0.5-2mm) ductile folds (Fig. 5h). These clasts are fine grained (~0.5mm) and are sub-rounded to rounded with a tabular shape (Figure 4d). The quartz appears as very fine-grained (~0.25mm) subhedral grains in thin bands (~0.5mm) with the hematite (Fig. 5f). The hematite is typically very fine grained (0.25mm) anhedral grains and rarely occurs as coarse-grained (~0.5mm) subhedral grains. The banded quartz hematite clasts display well defined banding (0.5-1mm thick) that is comprised of quartz rich and magnetite rich layers (Fig. 5g). The quartz rich layers are typically 60% quartz and 40% hematite and the hematite rich layers are typically 70% hematite and 30% quartz (Fig. 5g). Crosscutting the banding is a small (~1mm thick) coarse-grained (0.5mm) quartz vein (Fig. 5g). These clasts are fine grained (~0.5mm) and are sub-rounded with a tabular shape. The hematite is very fine-grained (~0.25mm) with an anhedral to subhedral shape and the quartz is very fine-grained (~0.25mm) with a subhedral shape.

The matrix can be divided into layered components; a specular hematite rich component and a hematite-quartz component (Figure 7). In hand specimen this layering is visible and there is no correlation between clast type and matrix type. Petrological analysis of the felsic matrix reveals lenses of tourmaline (Figure 6a), retrogressed sillimanite (Figure 6b), with minor muscovite and apatite. The tourmaline occurs as coarse grained (1-2mm) anhedral grains containing small (0.5mm) inclusions of hematite (Fig. 6c) and as symplectic intergrowths with fine grained (0.25mm) quartz (Figure 6a). Sillimanite occurs as small porphroblasts (~0.5mm) throughout the matrix and in some grains it displays low order birefringence colours (Fig. 6b). Minor coarse grained (~1mm) muscovite appears in the matrix, commonly with hematite. Coarse grained (~1mm) quartz is prominent in the felsic matrix and displays a subhedral shape with generally an inequigranular – polygonal texture and minor interlobate quartz grain boundaries. The magnetite rich matrix is comprised primarily of coarse grained (1-2mm) magnetite.

The conglomerate is interbedded with a psammite unit up to 2m thick and discontinuous throughout the outcrop due to poor exposure in places (Fig. 4e). The interbedded psammite consists of ~80% quartz with lesser magnetite, and minor sillimanite and tourmaline (Fig. 6d). The quartz is an anhedral shape with a seriate-interlobate texture. Grain size ranges from fine- to coarse-grain (0.5-2mm). Passive tabular cross-bedding is defined by a strong magnetite heavy mineral banding (Fig. 4f). Between individual sets of cross-beds is

recrystallise quartz displaying heterogeneously spaced patches of fine and coarse grains. This has deflected the forsets and primary bedding surfaces of the cross-bedding.

Balta Granite

The Balta Granite was first reported by Benbow and Flint (1979) and it is extensive throughout the Mount Woods Inlier (Chalmers 2007b). In the Spire Hills area, the granite comprises of a very coarse grain (20x10mm) phenocrysts of k-feldspar (red brick) and plagioclase in a groundmass of predominantly quartz with biotite and magnetite (Figure 4g). Throughout the inlier there are slight variants of the Balta Granite including a coarse grained porphyritic granite, a fine to medium grained granite, equigranular deep red granite and a clast rich variant (Chalmers 2007b).

Structural Elements

Skylark Metasediments

-First Generation Structures

The first generation foliation (S_{1s}) seen in the Skylark Metasediments is a gneissosity sub-parallel to compositional layering (S_0), it is pervasive throughout the small exposures of gneiss' (Fig. 4a,c). The S_1 foliation is defined by melanocratic layering in the gneiss and is commonly biotite–magnetite layering. Over the entire mapping area variations in the orientation of the S_1 foliation is evident. Due to the lack of exposure it is unclear how the variations relate.

-Second generation Structures

The second generation foliation (S_{2s}) seen in the Skylark Metasediments is a foliation defined by quartz-feldspar bands. This foliation (S_{2s}) is axial planar to small (2-5cm) F_2 folds formed from folding the S_{1s} foliation and defined by bands of alternating quartz-feldspar and magnetite-biotite layering (Fig. 4b).

Coodnambana Metaconglomerate

-First Generation Structures

Within the Coodnambana Metaconglomerate, the first generation foliation (S_{1c}) is best preserved within the interbedded psammite. S_{1c} is sub-parallel to compositional layering, and weakly preserved. In the interbedded psammite the S_{1c} foliation is defined by magnetite layering (Fig. 4f). Within the conglomerate the S_{1c} foliation is very weakly defined by the alignment of clasts.

-Second Generation Structures

The second generation foliation preserved in the Coodnambana Metaconglomerate is a pervasive fracture cleavage (S_f) (Fig. 4e). Within the conglomerate the second generation foliation is not preserved. The foliation is best preserved in the interbedded psammite as a discontinuous but pervasive fracture cleavage (Fig. 4e). Within the quartzite, the foliation is preserved as a discontinuous fracture cleavage. The S_f fracture cleavage is axial planar to a macroscopic scale synform that folds the quartzite and Coodnambana Metaconglomerate (Fig. 9). The synform plunges towards 294° with the southern limb dipping at 50° to the north (Fig. 10). The northern limb of the fold is covered with colluvium and as a result is not exposed. The effects of this folding event on the underlying Skylark Metasediments in uncertain, this is due to poor exposure of the Skylark Metasediments limiting any correlations between the two packages of rock.

-Faulting

Towards the northern extent of the fold sparse residual white quartz is present amongst the residual colluvium from the Skylark Metasediments. Over this area there is no visible continuity of the northern limb of the fold. This residual white quartz colluvium is aligned in a linear trace and trends at 140°. This implies that there is a fault present under the colluvium.

ZIRCON U-Pb GEOCHRONOLOGY

Sample Description

Two samples (SH001 and SH002) were collected from the Coodnambana Metaconglomerate outcrop at Spire Hills (Fig. 9). SH001 is a representative sample of the quartzite stratagraphically below the Coodnambana

Metaconglomerate (Fig. 9). The quartzite is suggested to be the lowest unit of the youngest stratigraphic sequence in the Mount Woods Complex (Fig. 8) (Betts *et al.* 2003, Chalmers 2007b). This sample was chosen to constrain a detrital or maximum depositional age of the youngest unit.

SH002 is representative of the Coodnambana Metaconglomerate and contains fine and coarse quartz clasts and metapsammitic clasts hosted within the mafic and felsic components of the matrix. This sample was chosen to constrain the maximum depositional age of the Coodnamabana Metaconglomerate and the provenance of the clasts. Two samples were extracted from sample SH002: SH002a and SH002b. Sample SH002a were two quartz-magnetite metapsammitic clasts (SH002a-1 and SH002a-2) separated from the matrix and other clasts, and were used to constrain the detrital age and provenance of the clasts. Sample SH002b was separated from the hematite-rich component of the matrix and was used to determine the maximum depositional and detrital age of the Coodnambana Metaconglomerate.

Geochronological Analysis

Zircon and monazite were separated at the University of Adelaide by standard crushing, milling, pan separation and heavy liquid techniques. Unsuccessful attempts were made to separate zircon from fine- and coarse-quartz clasts removed from the metaconglomerate. Zircon and monazite grains were mounted on epoxy discs. U-Th-Pb isotopic ratios were analysed using the laser ablation inductively coupled plasma-mass spectrometer (LA ICP-MS) at Adelaide Microscopy, University of Adelaide, South Australia. A beam size of 30µm was used and zircons between 50 to 100µm were targeted. For LA-ICP MS monazite analysis, a beam size of 12µm was used and monazites between 50 to 100µm were targeted.

Two zircon standards were analysed periodically in a separate mount during all zircon analyses for reference and calibration purposes. The zircon standards are “GJ-1” ($^{206}Pb/^{238}U$ = 600.7±1.1) and “Plesovice” ($^{206}Pb/^{238}U$ = 337.13±0.37). Three monazite standards were analysed: “222” ($^{206}Pb/^{238}U$ = 450.2±3.4), “440” ($^{206}Pb/^{238}U$ = 425) and “MAdel” ($^{206}Pb/^{238}U$ = 517.9±2.6). Data processing and reduction was undertaken using GEMOC and CSIRO’s GLITTER Data Reduction Software and ISOPLOT (Ludwig 2001, 2003).

Back Scattered Electron and Cathodoluminescence Imaging

Backscattered electron (BSE) and cathodoluminescence (CL) Imaging was undertaken on the Philips XL20 SEM at Adelaide Microscopy. This was used for identification of internal structures within the zircon and monazite.

SH001 – Quartzite

Zircon grains in this population range from 50 to 150µm in size and have a euhedral tabular to euhedral square prismatic shape (Fig. 11). The grains show oscillatory zoning under cathodeluminesence (Fig. 11). Within some grains there is a strong variation in the development of the oscillatory zones; this is seen particularly as a larger homogenious central zone (40µm) and external finer bands of alternating zones (3-4µm) (Fig. 11). Within some zircons the oscillatory zones are faded and appear blurred. Apparent in the CL images are fractures propagating through the grains.

SH002a-1 – Metapsammitic Clast

Zircon grains in this population range from 50 to 100µm in size and display a euhedral tabular to euhedral square prismatic shape (Fig. 12**Error! Reference source not found.**). Under cathodeluminesence alternating concentric bands are visible (Fig. 12). Within some grains there is a strong variation in the development of the oscillatory zones throughout the zircon; this is particularly evident within the larger homogeneous central zone (40µm) and generally finer banded oscillatory external zones. These oscillatory zones are variable in thickness (3-4µm to 10µm). Crosscutting the oscillatory zoning is a network of fractures.

SH002a-2 – Metapsammitic Clast

Zircon grains in this population range from 50 to 100µm in size and display a euhedral tabular to euhedral square prismatic shape (Fig. 13). Under cathodeluminesence alternating concentric bands are visible (Fig. 13). Within some grains there is a strong variation in the development of the oscillatory zones throughout the zircon; this is particularly evident within the larger homogeneous central zone (….µm) and generally finer banded oscillatory external zones. These oscillatory zones are variable in thickness (3µm to 10µm).

These two samples of the metapsammitic clast displayed similar zircon grain morphologies and grain shape and size. When analysed on the LA ICP-MS similar ages were collected (Table 2). The data from the two samples were combined in order to strengthen the statistics of the data set and the calculated age.

SH002b – Conglomerate Matrix

Monazite grains in this population are typically 50 to 100μm in diameter and generally have subhedral prismatic shape (Fig. 14). BSE images reveal a patchy zoning and homogeneous textures in the monazite grains. One monazite grain contained a brecciated texture with a vein of younger monazite within it. Within other monazite grains there are no visible textures.

Geochronology Results

SH001 – Quartzite

A total of 30 analyses from 18 zircon grains were collected for the SH001 sample; 28 analyses were used for the age calculation and one was discarded as it was a monazite grain (Table 1). Pb^{207}/Pb^{206} data show a slight positive skew suggesting there is a component of slightly older inherited material in the population. U-Pb data record a disconcordia with an upper intersect of 1729±18Ma and lower intersect of 51±130Ma (Fig. 15). A weighted average of the Pb^{207}/Pb^{206} data calculates an age of 1725±10Ma (MSWD=1.8, Probability = 0.006).

SH002a – Metapsammitic Clast

A total of 40 analyses from 26 zircon grains were collected from the sample SH002a; 35 analyses were used in the age calculation and five were discarded as they were monazite grains, heavily metamict zircon grains or were outside of two standard deviations (Table 2). Pb^{207}/Pb^{206} data show a unimodal age distribution and U-Pb record a disconcordia with an upper intercept of 1803±19Ma and lower intercept of -13±52Ma (MSWD = 0.79) (Fig. 16). A weighted average of the Pb^{207}/Pb^{206} data calculates an age of 1808±10Ma (MSWD=1.5, Probability 0.035), with two data points being omitted based on the points lying outside of two standard deviations.

SH002b – Metaconglomerate Matrix

A total of 26 analyses from 11 monazite grains were collected from the sample SH002b; 21 analyses were used for the age calculation and one analyses was discarded due to it being very disconcordant (Table 1). Pb^{207}/Pb^{206} data show two populations are apparent from Gaussian deconvolution; a population at 1559±9Ma of 21 spots and a population at 1594±10Ma of 4 spots (Fig. 17). All data points plot on the Concordia with a very slight negative disconcordance. A weighted average of the Pb^{207}/Pb^{206} data calculated an age of 1558±9Ma (MSWD=0.076, probability = 1).

The complete data for all three samples is within Appendix A.

DISCUSSION

Interpretation of U-Pb Geochronology

Quartzite

The U-Pb zircon age of the quartzite underlying the Coodnambana Metaconglomerate is 1725±10Ma (Fig. 15). These zircons all show oscillatory zoning indicating that they formed via magmatic processes and were later incorporated in the quartzite (Fig. 11). This age is interpreted as a maximum deposition age based on magmatic zircons being incorporated in a sedimentary rock. Individual spots show a strong population reflecting a unimodal age and with a single zircon spot at approximately 1850Ma (Fig. 15). A unimodal age indicates that the zircon grains were sourced from a unimodal magmatic source. Within the data set there are disconcordant analyses, these values plot to form a disconcordia with an intersect at 1725 Ma (Fig. 15). Concordant analyses plot around the 1725 Ma intercept and suggest that the 1725 Ma age is a reasonable approximation.

Coodnambana Metaconglomerate

The U-Pb zircon age of the quartz-magnetite metapsammitic clasts within the Coodnambana Metaconglomerate was 1808±10 Ma (Fig. 16). These zircons all show oscillatory zoning indicating that they formed via magmatic processes and was later incorporated within the metapsammitic rock (Fig. 12). This age is interpreted as a maximum depositional age based on magmatic zircons being incorporated into a sedimentary rock. Individual spots show a prominent unimodal population at 1808 Ma with three analyses ranging from 1960-2040 Ma (Fig. 16). This suggests that the zircon grains were sourced from a unimodal source and only show minor amounts

inherited recycled crust. Within the data set there are disconcordant analyses, these values plot to form a disconcordia which intersects at 1808 Ma (Fig. 16). Concordant analyses are seen plot around the 1808 Ma intercept and suggest that the 1808 Ma age is a reasonable approximation.

Monazite within the mafic matrix of the Coodnambana Metaconglomerate preserves a range of different textures. These textures include patchy zoning, a homogeneous texture and brecciated veins. Monazite can display a range of different textural zoning representing different geological events (Ayres *et al.* 1999). Patchy zoning is comprised of irregular shaped subequant zones that appear as embayments and fractures with variations in BSE response (Ayres *et al.* 1999) and has been suggested to develop due to overprinting of pre-existing monazite textures during *in situ* hydrothermal alteration (e.g. Poitrasson *et al.* 1996, Hawkins & Bowring 1997, Ayres *et al.* 1999). Hawkins & Bowring (1997) used TIMS U-Pb analysis to show that altered patchy zones within monazite grains in hydrothermally altered granite dyke consistently record a younger age than unaltered monazite within the same rock type. Monazite grains from the mafic matrix of the Coodnambana Metaconglomerate yield two ages of ~1590 Ma and 1558±9Ma (Fig. 17). The 1558 Ma age is seen within all three textures and the 1590 Ma age is only seen within the homogeneous monazite. The ~1590 Ma age is coeval with emplacement of the Balta Granite (ca. 1584, Fanning 1997a, Daly *et al.* 1998) and peak metamorphism (Forbes *et al.* in review); suggesting that this monazite was formed during the peak metamorphic event. Patchy and brecciated textures (fig. 14) are seen within the monazite grains and are interpreted as secondary textures representing hydrothermal alteration.

Source of the clasts within the Coodnambana Metaconglomerate

Identification of the source of the clasts within the Coodnambana Metaconglomerate has implications for the tectonostratigraphy of the Mount Woods Inlier. The clasts within the Coodnambana Metaconglomerate have been suggested to be sourced from the Skylark Metasediments (Betts *et al.* 2003, Chalmers 2007b). Betts *et al.* (2003) and Chalmers (2007b) based this interpretation on the clast lithologies being similar to various lithologies throughout the inlier such as metapsammites and quartzites. This interpretation implies that there must have been at least one metamorphic event prior to the deposition of the Coodnambana Metaconglomerate (Betts *et al.* 2003, Chalmers 2007b). This is based on metamorphosed clasts that preserve random orientations, implying

that they were metamorphosed during a prior event. An interbedded psammite within the Coodnambana Metaconglomerate yielded a U-Pb SHRIMP age of 1749±6Ma, which is suggested to approximate the age of the conglomerate matrix (Chalmers 2007b). This age is consistent with other detrital ages seen in the Skylark Metasediments; such as 1752±6 from the cordierite-biotite-garnet-sillimanite gneiss and 1749±6 from the cordierite-biotite-sillimanite gneiss (Fig. 18) (Chalmers, 2007). These ages are within error of each other and suggest that the metaconglomerate may have been sourced from the underlying Skylark Metasediments or the same source as the Skylark Metasediments.

Zircon grains analysed from the quartz-magnetite metapsammitic clast yield an age of 1808±10Ma. This age and detrital signature is significantly different from the detrital age of the interbedded psammite (ca. 1749 Ma, Chalmers 2007b) and the Skylark Metasediments (ca. 1752 Ma, Chalmers 2007b)(Fig. 18). As there is no detailed stratigraphy or geochronological resolution for the Skylark Metasediments it is unclear if the clasts were sourced from the Skylark Metasediments. Although, from the geochronology presented in this paper and published geochronology for the Skylark Metasediments the interpretation that the clasts were sourced from the Skylark Metasediments is not supported.

Betts (pers com) described a quartz-magnetite metapsamite at 'The Twins' exposure (Fig. 3) which may be a possible source rock for the metapsamitic clasts. There is no existing geochronology for this unit, so no comparisons between the metapsammitic clasts age and the psammite can be made. In addition, the Mount Woods Inlier contains other lithologies such as granitic intrusions and metapelites. Fine grained granitic clasts have been described by Chalmers (2007b) and these granitic clasts were not seen during structural mapping or in representative samples. Geochronology of such granitic clasts will provide better geochronological resolution for the Coodnambana Metaconglomerate and possibly aid in determining the source.

External to the Mount Woods Inlier zircon ages of ca. 1810 Ma are not common in Proterozoic terrains. Zircon ages within error of the ca. 1808 Ma age have been reported in the Ongeva Package in the Reynolds Ranges, Central Australia (Claoue-Long *et al.* 2008). This package contains a youngest statistically defined population with a mean age of 1808±5Ma and various detrital populations between 1840-2700Ma with a prominent population at ~2500Ma (Claoue-Long *et al.* 2008); the ~1808Ma age population is seen in the Metapelitic clast

and the older 1840-2700Ma detrital populations are not seen, implying that the Ongeva Package is unlikely to be the source of the metapsammitic clast.

It is unclear where the clasts in the Coodnambana Metaconglomerate were sourced from. The geochronology presented here does not support the hypothesis that the clasts in the Coodnambana Metaconglomerate were sourced from the Skylark Metasediments (Betts *et al.* 2003, Chalmers 2007b). As the geochronological resolution of the Skylark Metasediments is low this data does not disprove this interpretation. More geochronology of the Skylark Metasediments will improve this interpretation.

Hiatus in deposition between the Skylark Metasediments and Coodnambana Metaconglomerate

The contact between the quartzite at the base of the Coodnambana Metaconglomerate and the Skylark Metasediments is covered by colluvial sediments and not visible, therefore the nature of the contact cannot be directly attributed. Flint and Benbow (1977) describe the stratigraphic relationship of the Coodnambana Metaconglomerate and the underlying basement rock as unknown due to the lack of continuity of the exposure. Betts et al. (2003) and Chalmers (2007b) suggest that the Coodnambana Metaconglomerate unconformably overlies the Skylark Metasediments due to the interpretation that the clasts were sourced from the underlying Skylark Metasediments. Geochronological results presented here show that there is a significant difference in the maximum depositional ages between the Skylark Metasediments and quartzite. The Skylark Metasediments have a maximum depositional age of ca. 1752 Ma (Jagodzinski *et al.* 2007b, Chalmers 2007b) and the quartzite has a maximum depositional age of 1725±10 Ma, recording an age difference of 25 million years. This data indicates a hiatus in deposition between the Skylark Metasediments of at least 25 million years. However, as these ages are maximum depositional ages, imply that the Skylark Metasediments and the quartzite (and possibly the overlying Coodnambana Metaconglomerate) were deposited up to and possibly after ca. 1752 Ma and ca. 1725 Ma respectively. These maximum depositional are also close to or within error of the Kimban Orogeny (ca. 1.73-1.69 Ga, Hoek & Schaefer 1998, Vassallo & Wilson 2001), meaning that it is possible that one or both of the Skylark Metasediments and quartzite (and possibly Coodnambana Metaconglomerate) underwent deformation and metamorphism during the Kimban Orogeny.

The Skylark Metasediments and the quartzite/Coodnambana Metaconglomerate show evidence of deformation and metamorphism. Both units preserve a layer parallel foliation. Although, this layer parallel foliation is more strongly developed in the Skylark Metasediments. There is a distinct difference between the axial planar foliations seen between the two units. The Skylark Metasediments preserve melt segregations axial planar to the folds, while the interbedded psammite and quartzite preserve an axial planar cleavage. These are distinctly different structures and display a moderate difference in their orientations. Notably, due to the poor exposure of the Skylark Metasediments and the Coodnambana Metaconglomerate any relationship between the foliations is unclear. Ductile folding is clearly observed at the centimetre scale in the Skylark Metasediments, while folding at the metre scale is observed in the Coodnambana Metaconglomerate. Due to limited exposure the continuity of the metre scale folding and S_2 foliation in the Skylark Metasediments is unclear.

The relative timing of deformation in the Skylark Metasediments and the Coodnambana Metaconglomerate is unconstrained. It is unclear if the Skylark Metasediments underwent deformation prior to the deposition of the Coodnambana Metaconglomerate. The Coodnambana Metaconglomerate appears less deformed than the underlying Skylark Metasediments and this relationship has been interpreted as an unconformity. Treagus & Treagus (2002) and Czeck et al. (2009) found that the clast composition of a conglomerate (e.g. mafic, granitoid, quartzite) will influence the strain accommodation across different lithological domains. An example of this is seen in the Seine River Metaconglomerates, Ontaria, Canada where the heterogeneous distribution of the clast types (e.g. felsic volcanics, mafic volcanics, quartzites, banded iron formations) within the metaconglomerate has resulted in competency contrasts across the clast domains (Fissler *et al.* 2005a, b). Standard Fry and R_f/ϕ analysis was used to evaluate the strain recorded across each clast type and a clear variation in strain is seen at the regional scale (Fissler *et al.* 2005b). The variation is interpreted to be a difference in competence of each of the clast types and surrounding lithologies in the Seine River Metaconglomerate (Fissler *et al.* 2005a). Adjacent to the Seine River Metaconglomerate are metasediments that exhibit small to large scale shear zones and overall a significant variation in the accommodation of strain is seen across the region due to a single event (Fissler *et al.* 2005a).

The Coodnambana Metaconglomerate is predominately a clast supported polymictic conglomerate with a matrix composed of 80% magnetite and predominantly metapsammitic and quartzite clasts. A possible explanation of

why the Coodnambana Metaconglomerate appears only weakly deformed is a variation in the competency of the Coodnambana Metaconglomerate compared to the Skylark Metasediments. This interpretation does not require an unconformable contact between the two stratigraphic packages.

Within the Skylark Metasediments metamorphic grade is interpreted to be granulite facies (Betts et al., 2003; Chalmers, 2007b). This grade is well defined in the gt-cord-sp-sill pelite in which spinel and sillimanite is seen within cordierite cores which are in turn partially to completely rimed by garnet; this assemblage indicates granulite facies metamorphism (Chalmers, 2007b). Moonlight Hills which is suggested to be Skylark Metasediments by Chalmers (2007) experienced peak metamorphic conditions of ~4.7 kbar and 750 ^{o}C (Forbes *et al.,* in review).

The Coodnambana Metaconglomerate, interbedded psammite and basal quartzite all contain simple mineralogy due to an uncomplicated geochemistry. Sillimanite appears as small patches throughout the matrix of the Coodnambana Metaconglomerate, quartzite and interbedded psammite. The presence of sillimanite indicates that these rocks have reached at least upper amphibolite facies (Fig. 5a). Within the basal quartzite inclusions of andalusite are moated by fiberous sillimanite (Fig. 5a), reflecting the andalusite to sillimanite metamorphic reaction. This indicates that this package of rock experienced upper amphibolite facies metamorphism. Due to the simplicity of the geochemistry, key diagnostic mineral assemblages are not likely to grow and the Coodnambana Metaconglomerate may have reached a higher grade since the sillimanite field is a broad high temperature field. Timing of metamorphism in the Skylark Metasediments is based on a zircon crystallisation age of 1736±14 Ma from a first generation partial melt at Spire Hills (Finlay 1993, Fanning 1997a). The quality of this age is difficult to validate as there is no supplementary data describing the sample from which the zircons were taken, the morphology of the separated zircon grains or any imagery of the grains. Fanning (1993) reported that the uranium contents of these zircons are up to 740ppm and that these high uranium concentrations are unexpected for zircon grains that crystallised at granulite facies conditions (Fanning 1993). In general, zircons that crystallise under metamorphic conditions in the order of a few hundred parts per million and magmatic zircon contain uranium concentrations in the order of several hundred to about a thousand parts per million (Mezger & Krogstad 1997). The partial melt is likely to have formed from the Skylark Metasediments and inheritance of zircon is possible. The ca. 1736 Ma age has not been reproduced within the Mount Woods Inlier.

Ages within error of ca. 1736 Ma have been reported in the same sediments and have been shown to be magmatic ages. Without analysing the morphology of the 1736 Ma zircon grains, it is difficult to discern whether these are truly metamorphic zircon or if they represent magmatic zircon. There is no unequivocal evidence to determine if the Skylark Metasediments and the Coodnambana Metaconglomerate were metamorphosed during the same or different events.

Tectonic Models

Betts et al. (2003) proposed a complex evolutionary model for the Mount Woods Inlier involving multiple episodes of deformation, metamorphism and exhumation. In this model the Skylark Metasediments were deposited of the margin of an Archean continent. These sediments were metamorphosed and deformed during Kimban Orogeny (ca. 1.73-1.69 Ga, Hoek & Schaefer 1998, Vassallo & Wilson 2001), which resulted in development of isoclinal folds and a predominantly layer-parallel foliation. Betts et al. (2003) suggested that Kimban-aged deformation was associated with peak granulite facies metamorphic conditions. The Engenina Adamellite was emplaced post-Kimban at ca. 1692 (Fanning 1997a). The Mount Woods Inlier was then exhumed during the Early Kararan Orogeny (ca. 1.69-1.67 Ga, Daly *et al.* 1998), eroded and the Coodnambana Metaconglomerate was deposited as clastic sediments unconformably overlying the exhumed basement. The inlier was then reburied and underwent contact metamorphism by the Balta Granite (ca. 1584 Ma, Fanning 1997a). The inlier was then weakly deformed during the Late Kararan Orogeny (ca. 1.58-1.54 Ga, Daly *et al.* 1998) (Betts et al., 2003).

This model accounts for the unconformable contact between the Skylark Metasediments and the Coodnambana Metaconglomerate, and provides an explanation for why there is limited development of structural elements in the Coodnambana Metaconglomerate compared to the underlying Skylark Metasediments.

However, the model proposed by Betts et al. (2003) is reliant on the timing of metamorphism of the Skylark Metasdiments being ca. 1736 Ma, evidence of which is suggested to be the metamorphic zircon age from a partial melt within the Skylark Metasediments. As discussed earlier, there are uncertainties in the validity of this age and the age has not been repeatedly seen within the Mount Woods Inlier. However, other geochronological

studies conducted within the Mount Woods Inlier have revealed consistent U-Pb zircon metamorphic ages of ca. 1590 Ma (e.g., Jagodzinski *et al.* 2007b, Chalmers 2007b, Holm OZCHRON). Notably, only one phase of metamorphism is recorded at the Moonlight Hills exposure and peak metamorphism from this study has been suggested to occur at ca. 1590 Ma (Forbes *et al.* in review). It is currently unknown how the exposures of the Skylark metasediments at Moonlight Hills relate to the exposures at Spire Hills. Furthermore, the model is not directly supported by the new geochronology from the Coodnambana Metaconglomerate presented here, but the new data does not completely dismiss the model as a possibility.

The two-stage tectonothermal model proposed by Betts et al. (2003) is reliant on the metamorphosed clasts within the Coodnambana Metaconglomerate being sourced from the Skylark Metasediments, implying that the Skylark Metasediments were metamorphosed during an earlier event, then exhumed and incorporated as clasts into the Coodnambana Metaconglomerate. However, the new geochronological evidence from the Coodnambana Metaconglomerate suggests that the clasts were not sourced from the Skylark Metasediments. Implications of this are the Skylark Metasediments did not necessarily undergo a single of multiple phases of metamorphism before the deposition of the Coodnambana Metaconglomerate.

Holm (OZCHRON) has reported detrital components within the Mount Woods Inlier that have ages of 1652±22Ma of (sample 2003362532, Engenina 61 drill hole), 1670±13Ma (sample 2003362538, Engenina 38 drill hole) and 1627±19Ma (Engenina 61 drill hole). These clusters are interpreted to be a maximum provinence clusters (Holm, OZCHRON) and post date the Kimban Orogeny (Neumann & Frasier 2007). Meaning that these sedimentary packages were deposited after the Kimban aged metamorphism and deformation and could not have been metamorphosed or deformed by the Kimban Orogeny. Notably the Engenina Adamellite (1692±25Ma, Fanning 1997b, Daly *et al.* 1998) intrudes the Skylark Metasediments (Benbow & Flint 1979, Betts *et al.* 2003) and these maximum provenance clusters post date the Engenina Adamellite (Neumann & Frasier 2007). Neumann & Fraser (2007) describe that there must be a pre- ~1690Ma sedimentary package based on the Engenina Adamellite intruding these packages (Benbow & Flint 1979, Betts *et al.* 2003) and a post- ~1670Ma package based on younger maximum provenance cluster (Holm, OZCHRON). The nature of these two sedimentary packages is unclear and Neumann & Fraser (2007) suggest that the younger package may correlate with the Coodnambana Metaconglomerate. Two interpretations can be made from these maximum

provenance clusters: that the Mount Woods Inlier was deposited in two sedimentary cycles or that it was deposited in a continuous sedimentary cycle in which the lower parts of the sequence were intruded by the Engenina Adamellite while the upper parts of the sequence were being deposited. This has been seen in the Moine Supergroup where intruded granites yield ages coeval with volcanic tuffs suggesting that the granites were anorogenic intrusives during a rift phase (Kinny *et al.* 2003).

The timing of metamorphism is a crucial issue in the Mount Woods Inlier. As discussed earlier, there are uncertainties with the ca. 1736 Ma metamorphic age. Forbes *et al.* (in review) has suggested that the Mount Woods Inlier experienced only one metamorphic event and suggested that it occurred at ca. 1590 Ma. Meaning that if the Mount Woods Inlier only experienced one phase of metamorphism sedimentation may have occurred in a continuous basin from ca. 1750 Ma to 1630 Ma and possibly 1590 Ma.

We propose an alternate single-stage depositional and tectonothermal model for the Mount Woods Inlier based on the geochronological data present here and recently published geochronology. We suggest that the sediments of the Mount Woods Complex were deposited in a continuous sedimentary basin from ca. 1750 Ma to at least 1630 Ma, and possibly up to 1590 Ma. During deposition the lower portions of the stratigraphy were intruded by the Engenina Adamellite at ca. 1692 Ma where the pre-1692 Ma sediments were intruded and the later ca. 1690-1590 Ma sediments were deposited after the intrusion. Sedimentation ceased at approximately 1590 Ma with the onset of the 1590 Ma Event; possibly related to the Olarian or Isan Orogeny's. During this event the sediments were deformed and metamorphosed to upper amphibolite to granulite facies. Deformation is expressed as isoclinals folding and the development of shear zones. Metamorphic conditions were approximately ~4.7 kbar and 750^{o}C (Forbes *et al.* in review). At ca. 1558 Ma the Mount Woods Inlier experienced a hydrothermal event.

Further work is needed in the Mount Woods Inlier to support this model. The geochronological resolution of the Mount Woods Inlier is low and currently geochronological data is only available for a select few units. Further geochronology of the sedimentary units is likely to provide a better insight to the evolution of the Mount Woods Inlier. Other useful work includes calculating the P-T histories for other exposures in the Mount Woods Inlier. This would be useful in terms of understanding the metamorphic evolution in other parts of the stratigraphy and

particularly useful at the Spire Hills exposure where the evidence for Kimban-aged metamorphism has been reported. This will investigate whether Spire Hills experienced a single or multiple metamorphic events. Furthermore, a better geochronological understanding may lead to correlations between other Eastern Proterozoic terrains such as the Broken Hill Block which contains similar depositional (ca. 1800-1710 Ma, ca. 1710-1660 Ma, ca. 1660-1600 Ma) and metamorphic ages (ca. 1590) (Page *et al.* 2000a, Raetz *et al.* 2002).

CONCLUSION

The U-Pb zircon and monazite geochronology from the Coodnambana Metaconglomerate indicates that the sediments and clasts were not sourced from the Skylark Metasediments. This implies that the Mount Woods Inlier did not necessarily experience a pre-1590 Ma metamorphic event and does not imply the presence of an unconformity between the Skylark Metasediments and the Coodnambana Metaconglomerate. We propose an alternate single stage depositional and tectonothermal model for the Mount Woods Inlier. Further work to strengthen this model is needed and may lead to correlations with other Eastern Proterozoic terrains.

REFERENCES

AMBROSE G. J. & FLINT R. B. 1981. BILLA KALINA, South Australia. *Geological Survey of South Australia geological notes*.

AYRES J. C., MILLER C., GORISCH B. & MILLEMAN J. 1999. Textural development of monazite during high-grade metamorphism: Hydrothermal growth kinetics, with implications for U, Th-Pb geochronology. *American Mineralogist* **84**, 1766-1780.

BENBOW M. C. & FLINT R. B. 1979. The Engenina Adamellite and Balta Granite of the Mount Woods Inlier. *The Geological Survey of South Australia Quaterly Geological Notes no. 69*, 9-13.

BETTS P. G., GILES D., LISTER G. S. & FRICK L. R. 2002. Evolution of the Australian Lithosphere. *Australian Journal of Earth Science* **49**, 661 - 695.

BETTS P. G., VALENTA R. K. & FINLAY J. 2003. Evolution of the Mount Woods Inlier, northern Gawler Craton, Southern Australia: an integrated structual and aeromagnetic analysis. *Tectonophysics* **366**, 83 - 111.

BLACK L. P., GREGORY P., WITHNALL I. W. & BAIN J. H. C. 1998. U-Pb zircon are for the Etheridge Group, Georgetown region, north Queensland: implications for relationship with the Broken Hill and Mt Isa sequences. *Australian Journal of Earth Science* **45**, 925-935.

CHALMERS N. C. 2007a. The Mount Woods Domain: a geological review and discussion on mineralisation potential. *Department of Primary Industries and Resources South Australia Roport Book 2007/7*, 67pp.

CHALMERS N. C. 2007b. Mount Woods Domain: Proterozoic Metasediments and intrusives. *department of Primary Industries and Resources South Australia Roport Book 2007/20*, 78pp.

CLAOUE-LONG J., EDGOOSE C. & WORDEN K. 2008. A correlation of Aileron Province stratigraphy in central Australia. *Precambrian Research* **166**, 230-145.

CREASER R. A. & COOPER J. A. 1993. U-Pb geochronology of middle Proterozoic felsic magmatism surrounding the Olympic Dam Cu-U-Au-Ag and Moonta Cu-Au-Ag deposits, South Australia. *Economic Geology* **88**, 186-197.

CREASER R. A. & WHITE A. J. R. 1991. Yardea Dacite; large-volume, hightemperature felsic volcanism from the middle Proterozoic of South Australia. *Geology* **19**, 48-51.

CZECK D. M., FISSLER D. A., HORSMAN E. & TIKOFF B. 2009. Strain analysis and rheology contrasts in polymictic conglomerates: An example from the Seine metaconglomerates, Superior Province, Canada. *Journal of Structural Geology* **31**, 1365-1376.

DALY S. J., FANNING C. M. & FAIRCLOUGH M. C. 1998. Tectonic evolution and exploration potential of the Gawler Craton, South Australia. *Abstracts Geological Society of Australia* **49**, 104.

ELBURG M. A., BONS P. D., DOUGHERTY-PAGE J., JANKA C. E., NEUMANN N. L. & SCHAEFER B. F. 2001. Age and metasomatic alteration of the Mt Neill Granite at Nooldoonooldoona Waterhole, Mt Painter Inlier, South Australia. *Australian Journal of Earth Science* **48**, 721 - 730.

FANNING C. M. 1993. Ion-microprobe U-Pb Zircon Dating of the Mount Woods Inlier, Preliminary results. *Personal Communication*.

FANNING C. M. 1997a. Geochronological synthesis of southern Australia: Part II, The Gawler Craton, South Australia. *Department of Primary Industries and Resources. Open file envelope 08918, Adelaide*, 46pp.

FANNING C. M. 1997b. Geochronological Synthesis of Southern Australia: Part II. The Gawler Craton South Australia. *Department of Mines and Energy Open File Envelope 88918 (unpublished)*.

FINLAY J. 1993. Structural Interpretation in the Mount Woods Inlier. *Unpublished Honours Thesis*.

FISSLER D. A., CZECK D. M. & HORSMAN E. 2005a. Quantifying strain in various lithologies and documenting a strain gradient within the Seine River Basin, northwestern Ontario, Canada *Geological Society of America Abstracts with Programs* **37**, 212.

FISSLER D. A., CZECK D. M. & HORSMAN E. 2005b. A quantitative analysis of strain in the Seine River Metaconglomerates, Rainy Lake Region, northern Ontario, Canada. *Geological Society of America Abstracts with Programs* **37**, 29.

FLINT R. B. & BENBOW M. C. 1977. Geology of the Mount Woods Inlier. *South Australian Department of Mines and Energy Report 77/134*.

FORBES C. J., BETTS P. G., GILES D. & WEINBERG R. 2008. Reinterpretation of the tectonic context of high-temperature metamorphism in the Broken Hill Block, NSW, and implications on the Palaeo- to Meso-Proterozoic evolution. *Precambrian Research* **166**, 338 - 349.

FORBES C. J., GILES D., HAND M., BETTS P. G., CHALMERS N. C. & DUTCH R. in review. Using P-T paths to interpret the tectonothermal setting of prograde metamorphism: an example from the northeastern Gawler Craton, South Australia.

GILES D., BETTS P. & LISTER G. 2002. Far-field continental backarc setting for the 1.80–1.67 Ga basins of northeastern Australia. *Geology* **30**, 823 - 826.

GILES D. & NUTMAN A. P. 2002. SHRIMP U-Pb monazite dating of 1600-1580 Ma amphibolite facies metamorphism in the southeastern Mt Isa Block, Australia. *Australian Journal of Earth Science* **49**, 455 - 465.

HAWKINS D. P. & BOWRING S. A. 1997. U-Pb systematics of monazite and xenotime: case studies from the Paleoproterozoic of the Grand Canyon, Arizona. *Contributions to Mineral Petrology* **127**, 87-103.

HOEK J. D. & SCHAEFER B. F. 1998. Palaeoproterozoic Kimban mobile belt, Eyre Peninsula; timing and significance of felsic and mafic magmatism and deformation. *Australian Journal of Earth Sciences* **45**, 305-313.

HOLM O. OZCHRON. OZCHROM - SHRIMP Interpretive Pooled Age Report. *Geoscience Australia SHRIMP U-Pb Geochronology Interim Data Release July 2007*.

JAGODZINSKI E. A., REID A. J., CHALMERS N., SWAIN G., FREW R. A. & FOUDOULIS C. 2007a. Compilarion of SHRIMP U-Pb geochronological data for the Gawler Craton, South Australia, 2007. *Department of Primary Industries and Resources Report Book 2007/21*.

JAGODZINSKI E. A., REID A. J., CHALMERS N. C., SWAIN G., FREW R. A. & FOUDOULIS C. 2007b. Compilation of SHRIMP U-Pb geochronological data for the Gawler Craton, South Australia, 2007. *Department of Primary Industries and Resources South Australia Roport Book 2007/21*.

KINNY P. D., STRACHAN R. A., KOCKS H. & C.R.L. F. 2003. U-Pb geochronology of late Neoproterozoic augen granites in the Moine Supergroup, NW Scotland: dating of rift-related, felsic magmatism during supercontinent break-up? *Journal of the Geological Society of Australia.* **160**, 925-934.

LUDWIG K. R. 2001. Users manual for Isoplot/Ex (rev. 2.49): A geochronological toolkit for Microsoft Excel. *Berkeley Geochronology Center Special Publication*.

LUDWIG K. R. 2003. User's manual for Isoplot 3.00: a geochronological toolkit for Microsoft Excel. *Berkeley Geochronology Center Special Publication*.

MEZGER K. & KROGSTAD E. J. 1997. Interpretation of disconcordant U-Pb zircon ages: An evaluation. *Journal of Metamorphic Geology* **15**, 127-140.

NEUMANN N. L. & FRASIER G. L. 2007. Geochronological synthesis and Time-Space plots for Proterozoic Australia. *Geoscience Australia Record 2007/06*.

PAGE R. W., JACKSON M. J. & KRASSAY A. A. 2000b. Constraining sequence stratigraphy in north Australian basins: SHRIMP U-Pb zircon geochronology between Mt Isa and McArthur River. *Australian Journal of Earth Science* **47**, 431–459.

PAGE R. W., STEVENS B. J. P., GIBSON G. M. & CONOR C. H. 2000a. Geochronology of Willyama Supergroup rocks between Olary and Broken Hill, and comparison to northern Australia. *Australian Geological Survey Organisation Record* **2000/10**, 72-75.

POITRASSON F., CHENERY S. & BLAND D. J. 1996. Contrasted monazite hydrothermal alteration mechanisms and their geochemical implications. *Earth and Planetary Science Letters* **145**, 79-96.

RAETZ M., KRABBENDAM M. & DONAGHY A. G. 2002. Compilation of U-Pb zircon data from the Willyama Supergroup, Broken Hill region, Australia: evidence for three tectonostratigraphic successions and four magmatic events? *Australian Journal of Earth Science* **49**, 965-983.

RAWLINGS D. J. 1999. Stratigraphic resolution of a multiphase intracratonic basin system: the McArthur Basin, northern Australia. *Australian Journal of Earth Science* **46**, 703 - 723.

SCOTT D. L., RAWLINGS D. J., PAGE R. W., TARLOWSKI C. Z., IDNURM M., JACKSON M. J. & SOUTHGATE P. N. 2000. Basement framework and geodynamic evolution of the Palaeoproterozoic superbasins of north-central Australia; an integrated review of geochemical, geochronological and geophysical data. *Australian Journal of Earth Sciences* **47**, 341 -380.

TREAGUS S. H. & TREAGUS J. E. 2002. Studies of strain and rheology of conglomerates. *Journal of Structural Geology* **24**, 1541-1567.

VASSALLO J. J. & WILSON C. J. L. 2001. Structural repetition of the Hutchison Group metasediments, Eyre Peninsula, South Australia. *Australian Journal of Earth Sciences* **48**, 331-345.

WADE B. P., KELSEY D. E., HAND M. & BAROVICH K. M. 2008. The Musgrave Province: Stitching north, west and south Australia. *Precambrian Research* **166** 370 - 386.

WITHNALL I. W., BAIN J. H. C., J.J. D., D.E. M. & B.S. O. 1988. Proterozoic stratigraphy and tectonic history of the Georgetown Inlier, Northeastern Queensland. *Precombrian Research* **40/41**, 429 - 446.

WYBORN L. 1998. Younger ca 1500 Ma granites of the Williams and Naraku Batholiths, Cloncurry district, eastern Mt Isa Inlier: geochemistry, orogin, metallogenic significance and explortaion indicators. *Australian Journal of Earth Science* **45**, 397 - 411.

FIGURE AND TABLE CAPTIONS

Figure 1 – Map of Eastern Proterozoic Australia and the location of the Mount Woods Inlier and other Eastern Proterozoic terrains. Courtesy of Caroline Forbes

Figure 2 – TMI image of the Mount Woods Inlier overlain with maximum depositional and detrital ages throughout the Mount Woods Inlier (Chalmers 2007b, Jagodzinski 2007, Holm OZCHRON), structural features from Betts et al., 2003

Figure 3 – TMI image of the Mount Woods Inlier overlain with basement rock exposures. Structural features from Betts et al., 2003

Figure 4 – Outcrop photos from the Coodnambana Metaconglomerate exposure. a) strained cord-feld gneiss b) centimetre scale folds in cord-feld gneiss c) highly strained psammite d) fine-grained and metapsammitic clasts within hematite matrix, Coodnambana Metaconglomerate e) fracture cleavage within interbedded psammite f) tabular crossbedding in the interbedded psammite g) Balta Granite adjacent to the Coodnambana Metaconglomerate

Figure 5 – Photomicrographs. a) andalusite-sillimanite porphyroblast in quartzite b) pinning microstructure in quartzite c) undulosed extinction of quartz grain of the quartzite d) retrogressed sillimanite in quartzite e) quartz grains within coarse-grained quartz clast f) millimetre scale folds in metapsammitic clast g) quartz-hematite layers in metapsammitic clast with melt vein h) coarse-grained folded quartz vein in metapsammitic clast

Figure 6 – Photomicrographs. a) symplectic intergrowth of quartz-tourmaline in the conglomerate matrix b) sillimanite within conglomerate matrix c) coarse-grained tourmaline and hematite within the conglomerate matrix d) coarse-grained quartz grains and sillimanite in the interbedded psammite

Figure 7 – Slice through the Coodnambana Metaconglomerate showing alternating layers of mafic and felsic matrix

FIGURES AND TABLES

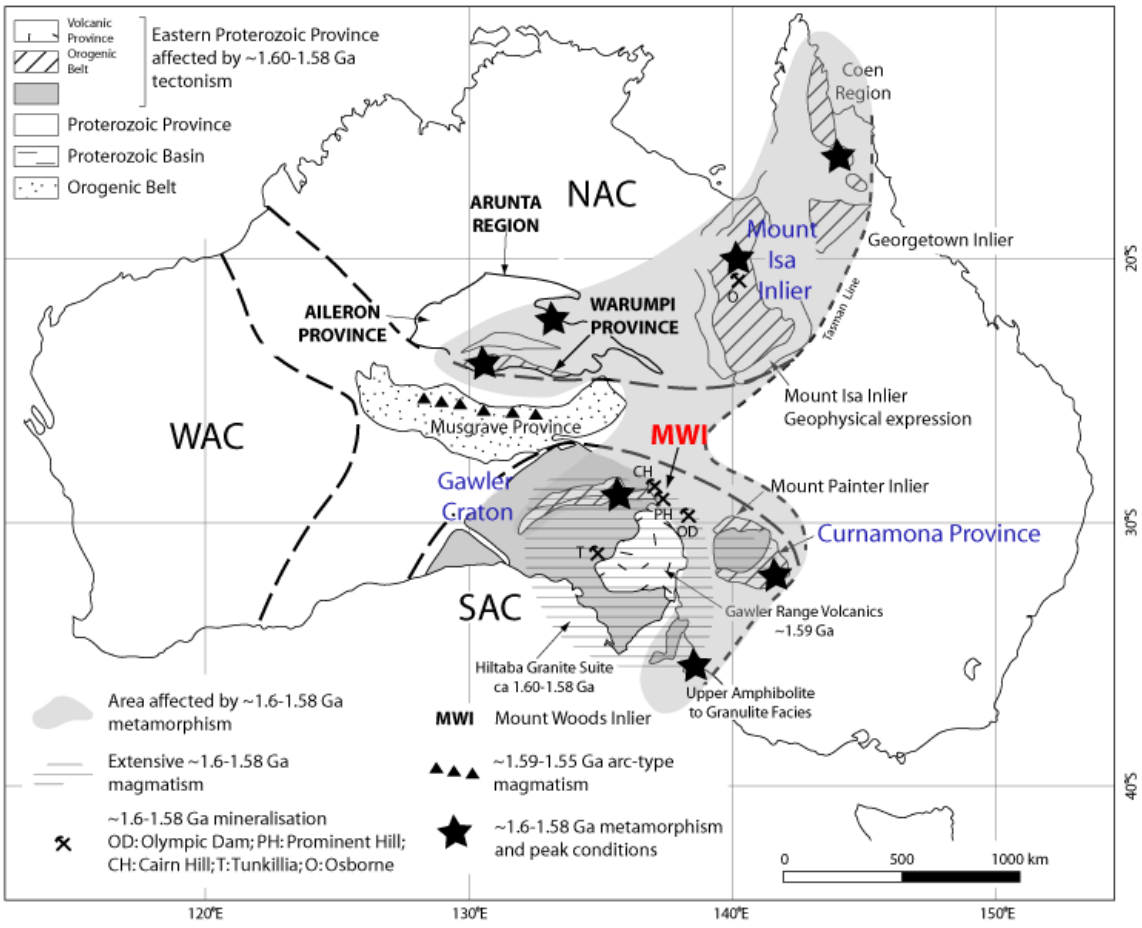
Volcanic Province
Orogenic Belt
Eastern Proterozoic Province affected by ~1.60-1.58 Ga tectonism
Proterozoic Province
Proterozoic Basin
Orogenic Belt
Coen Region
ARUNTA REGION
NAC
Mount Isa Inlier
Georgetown Inlier
AILERON PROVINCE
WARUMPI PROVINCE
Taman Line
Mount Isa Inlier Geophysical expression
WAC
Musgrave Province
MWI
Gawler Craton
CH
PH
OD
T
O
Mount Painter Inlier
Curnamona Province
SAC
Gawler Range Volcanics ~1.59 Ga
Hiltaba Granite Suite ca 1.60-1.58 Ga
Upper Amphibolite to Granulite Facies
Area affected by ~1.6-1.58 Ga metamorphism
Extensive ~1.6-1.58 Ga magmatism
~1.6-1.58 Ga mineralisation
OD: Olympic Dam; PH: Prominent Hill; CH: Cairn Hill; T: Tunkillia; O: Osborne
MWI Mount Woods Inlier
~1.59-1.55 Ga arc-type magmatism
~1.6-1.58 Ga metamorphism and peak conditions
0 500 1000 km
120°E
130°E
140°E
150°E
20°S
30°S
40°S

Figure 1

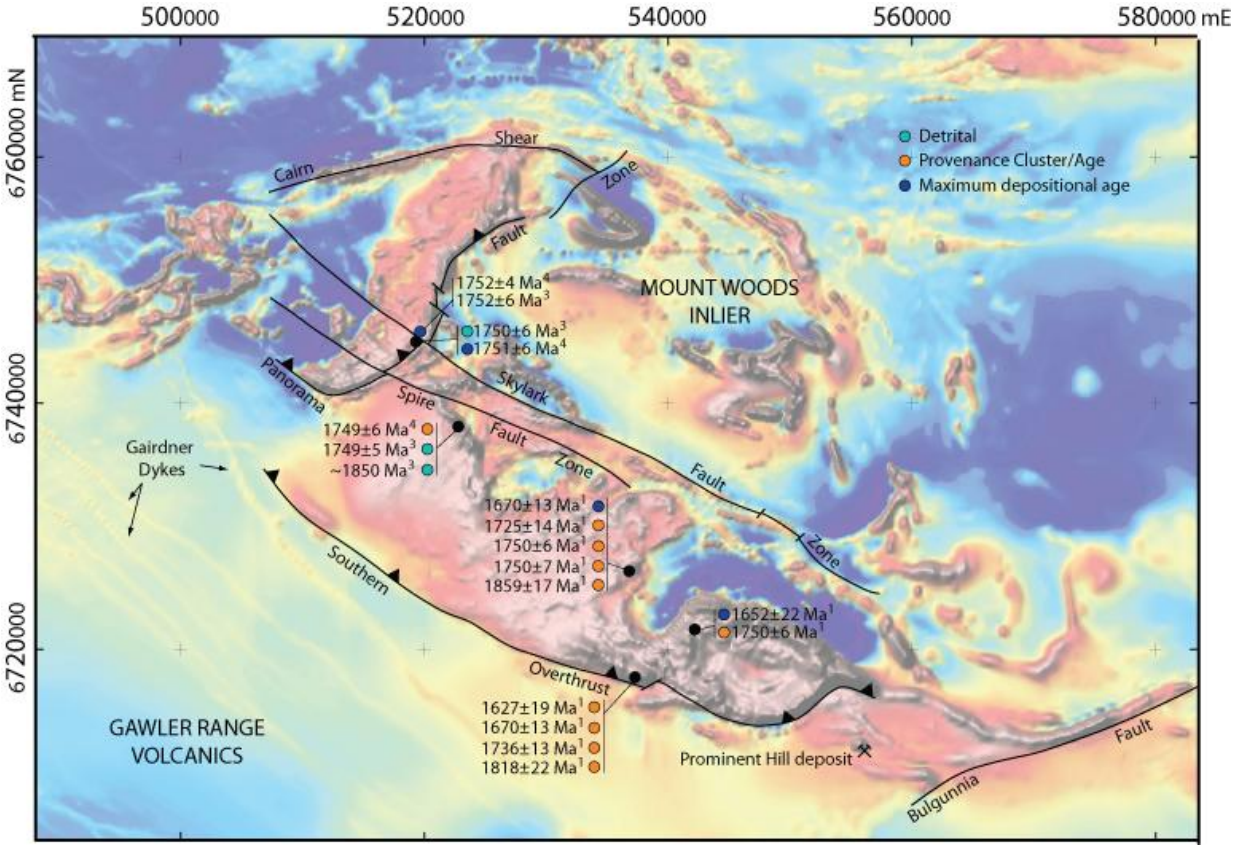
500000
520000
540000
560000
580000 mE
6760000 mN
6740000
6720000
Detrital
Provenance Cluster/Age
Maximum depositional age
Cairn
Shear
Zone
Fault
1752±4 Ma4
1752±6 Ma3
MOUNT WOODS
INLIER
1750±6 Ma3
1751±6 Ma4
Panorama
Spire
Skylark
1749±6 Ma4
1749±5 Ma3
~1850 Ma3
Fault
Zone
Gairdner
Dykes
Fault
1670±13 Ma1
1725±14 Ma1
1750±6 Ma1
1750±7 Ma1
1859±17 Ma1
Zone
Southern
1652±22 Ma1
1750±6 Ma1
Overthrust
1627±19 Ma1
1670±13 Ma1
1736±13 Ma1
1818±22 Ma1
GAWLER RANGE
VOLCANICS
Prominent Hill deposit
Fault
Bulgunnia

Figure 2

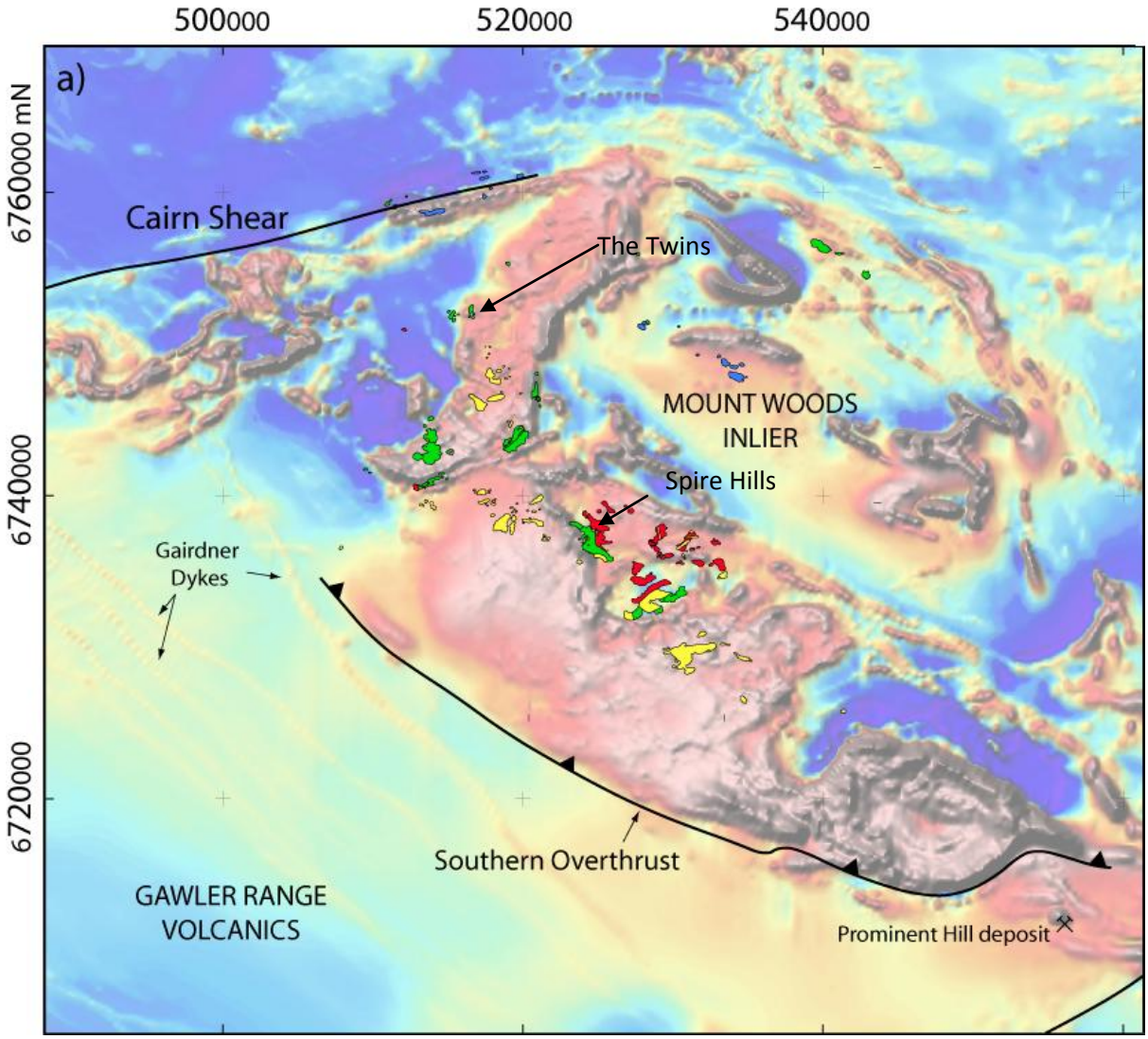
500000
520000
540000
a)
6760000 mN
6740000
6720000
Cairn Shear
The Twins
MOUNT WOODS
INLIER
Spire Hills
Gairdner
Dykes
Southern Overthrust
GAWLER RANGE
VOLCANICS
Prominent Hill deposit

Figure 3

Figure 4

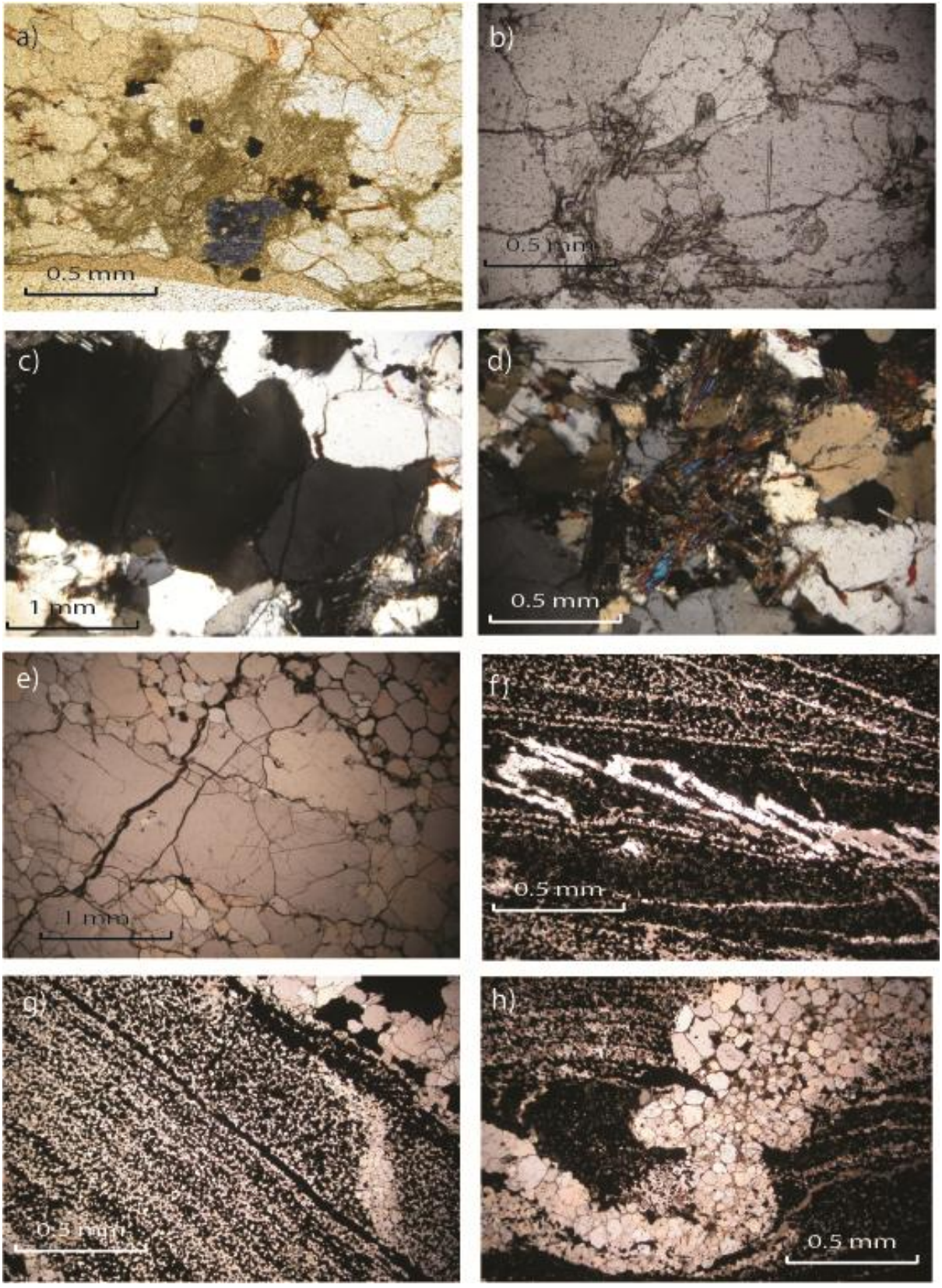

Figure 5

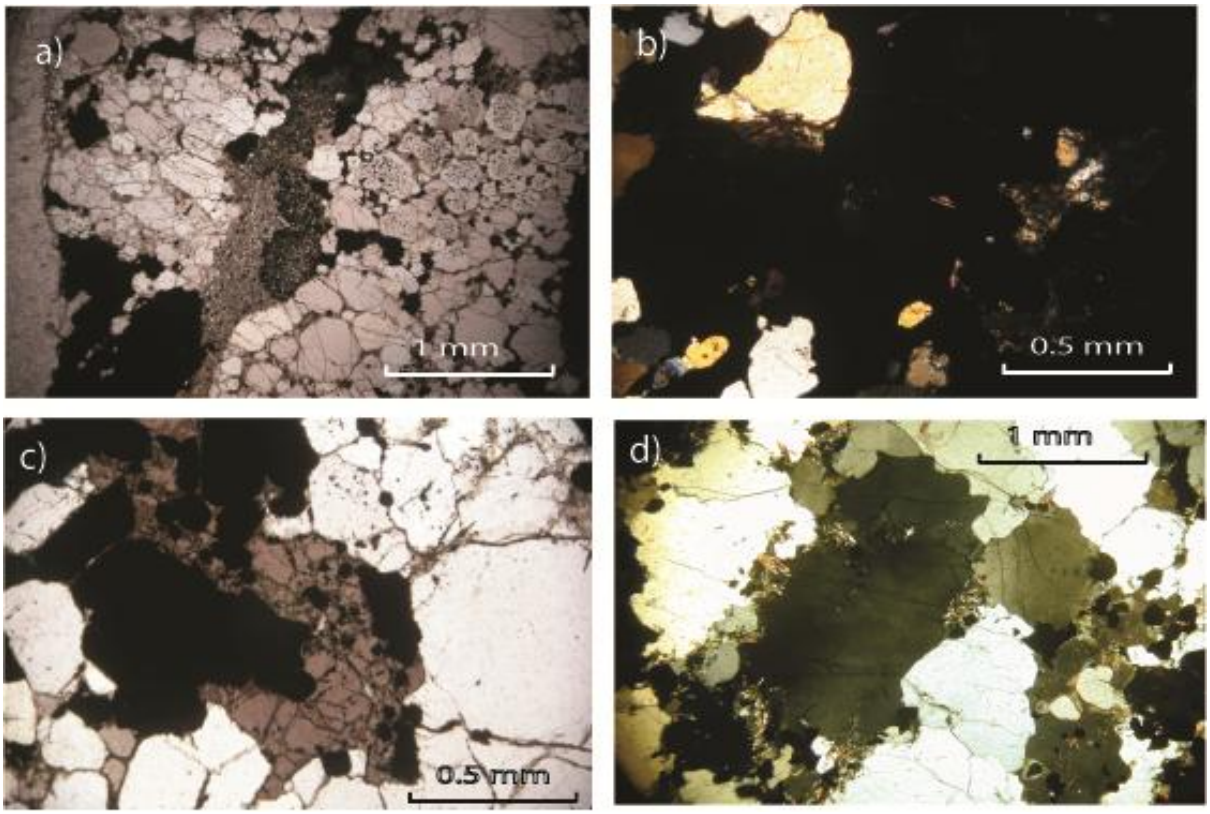

Figure 6

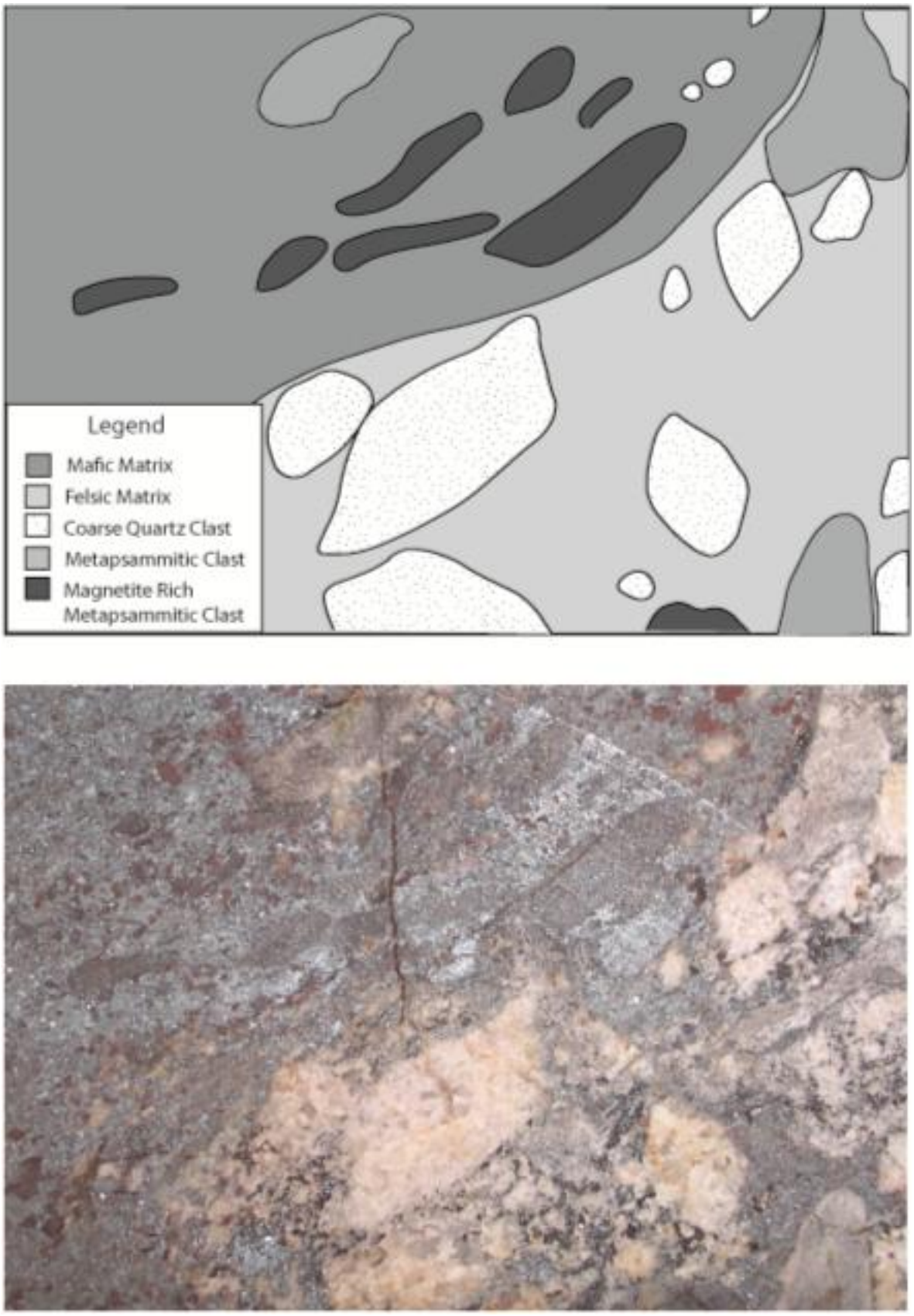
Legend
Mafic Matrix
Felsic Matrix
Coarse Quartz Clast
Metapsammitic Clast
Magnetite Rich
Metapsammitic Clast

Figure 7

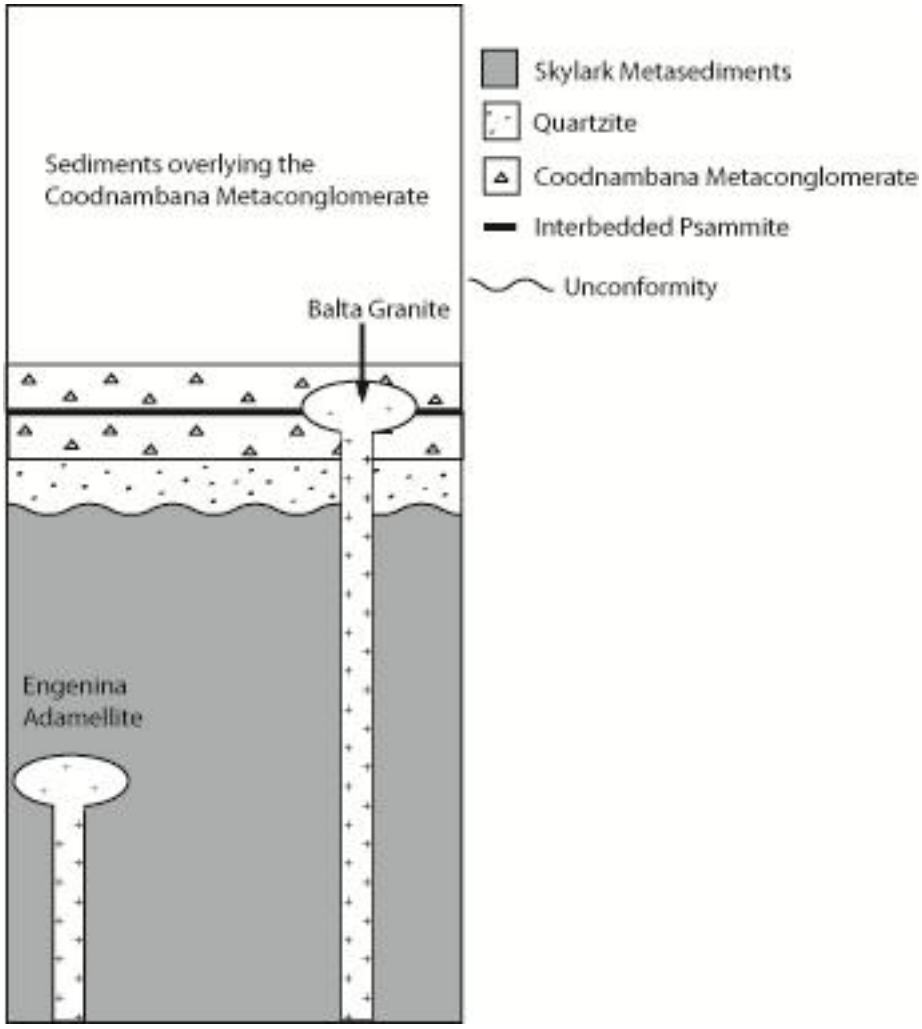
Sediments overlying the
Coodnambana Metaconglomerate
Balta Granite
Engenina
Adamellite
Skylark Metasediments
Quartzite
Coodnambana Metaconglomerate
Interbedded Psammite
Unconformity

Figure 8

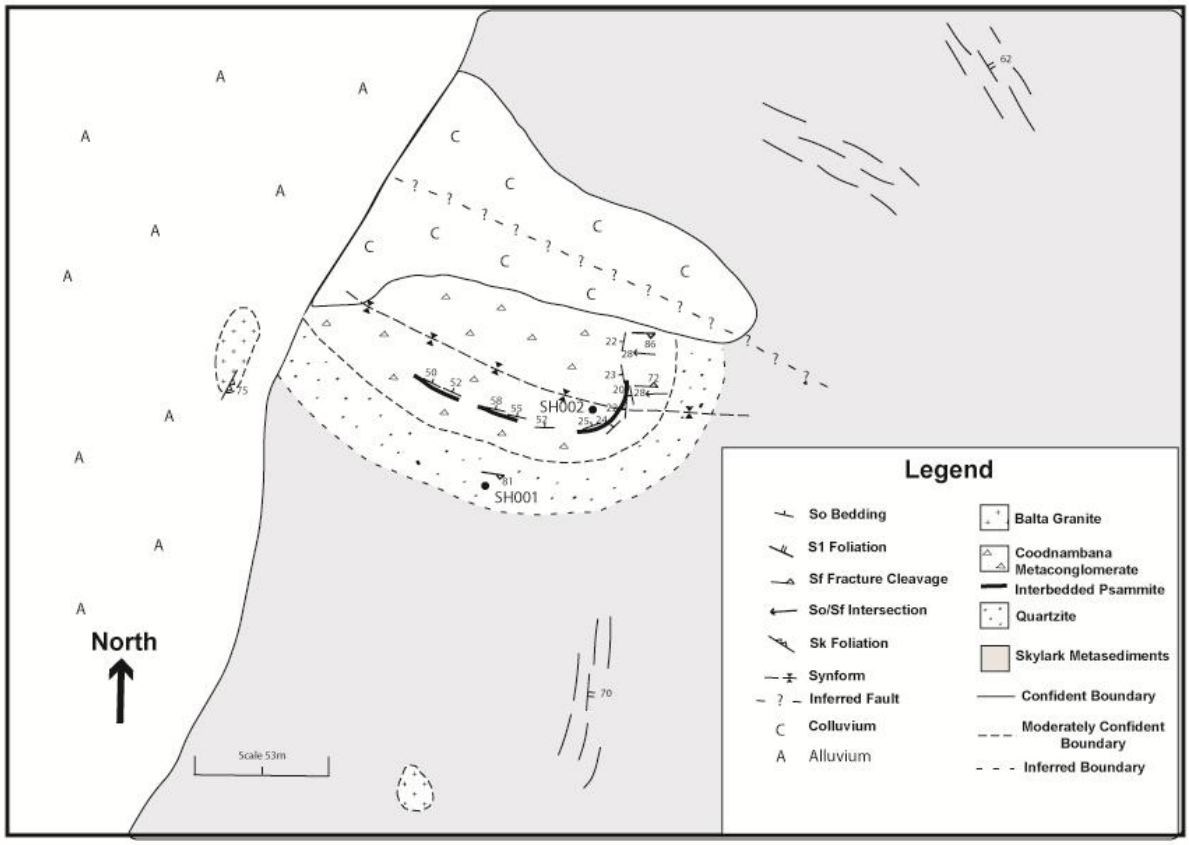
A
C
SH002
SH001
North
Scale 53m
Legend
So Bedding
S1 Foliation
Sf Fracture Cleavage
So/Sf Intersection
Sk Foliation
Synform
Inferred Fault
Colluvium
Alluvium
Balta Granite
Coodnambana Metaconglomerate
Interbedded Psammite
Quartzite
Skylark Metasediments
Confident Boundary
Moderately Confident Boundary
Inferred Boundary

Figure 9

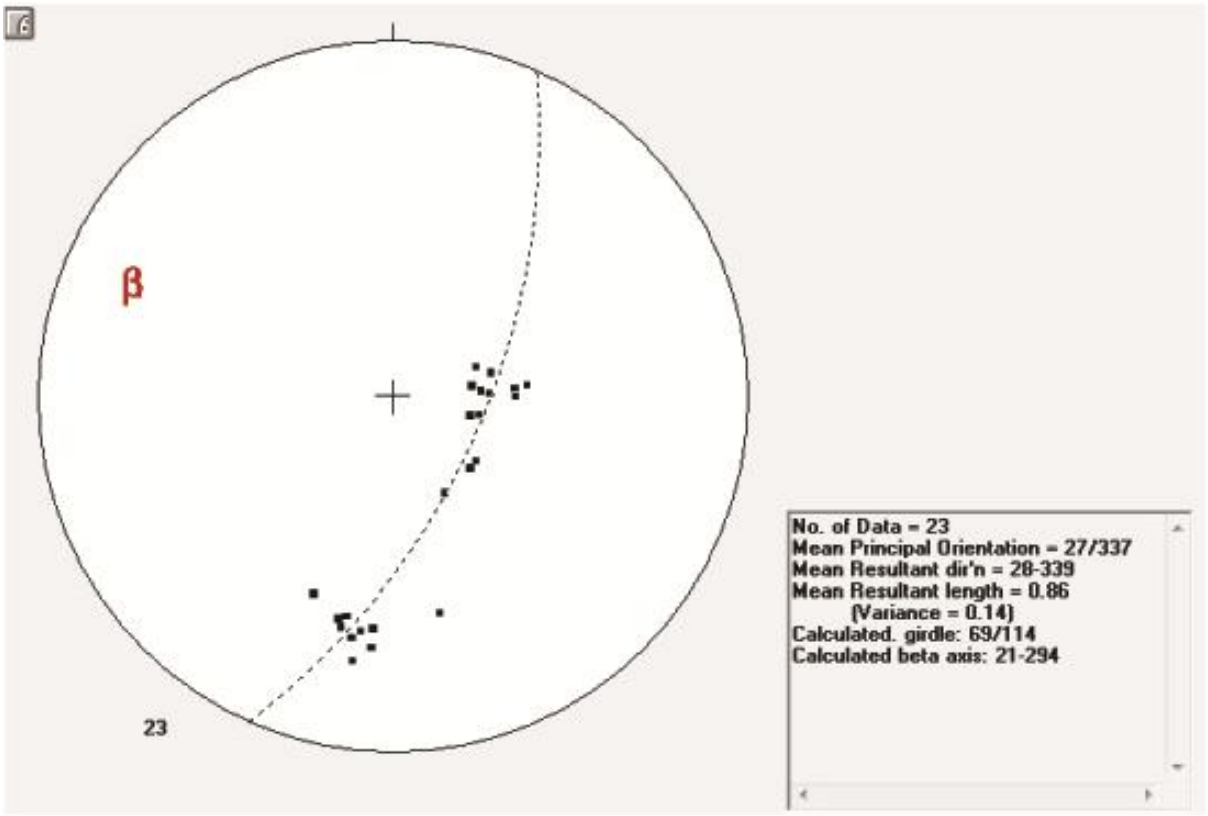
β
23
No. of Data = 23
Mean Principal Orientation = 27/337
Mean Resultant dir'n = 28-339
Mean Resultant length = 0.86
(Variance = 0.14)
Calculated. girdle: 69/114
Calculated beta axis: 21-294

Figure 10

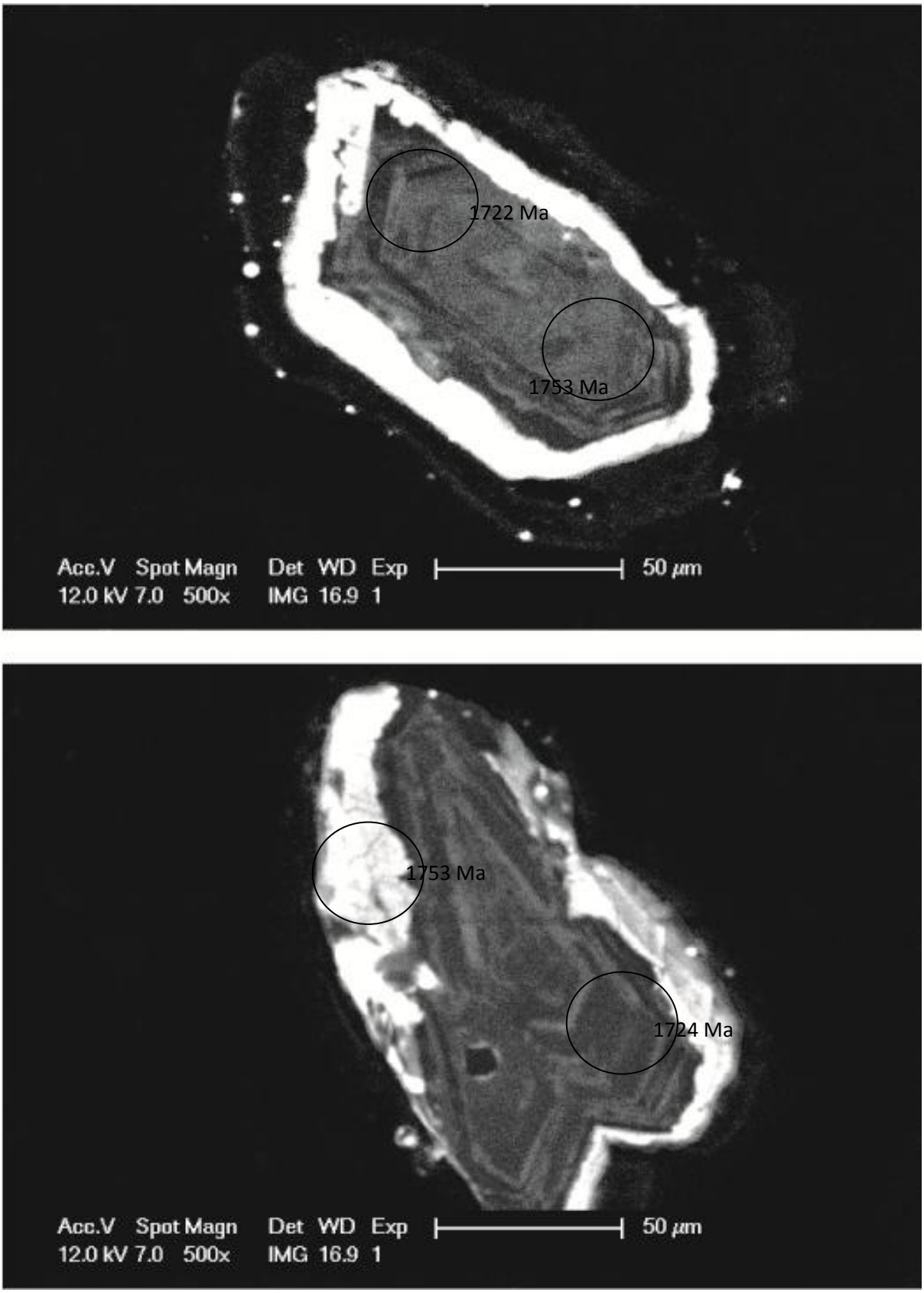
1722 Ma
1753 Ma
Acc.V Spot Magn Det WD Exp 50 µm
12.0 kV 7.0 500x IMG 16.9 1
1753 Ma
1724 Ma
Acc.V Spot Magn Det WD Exp 50 µm
12.0 kV 7.0 500x IMG 16.9 1

Figure 11

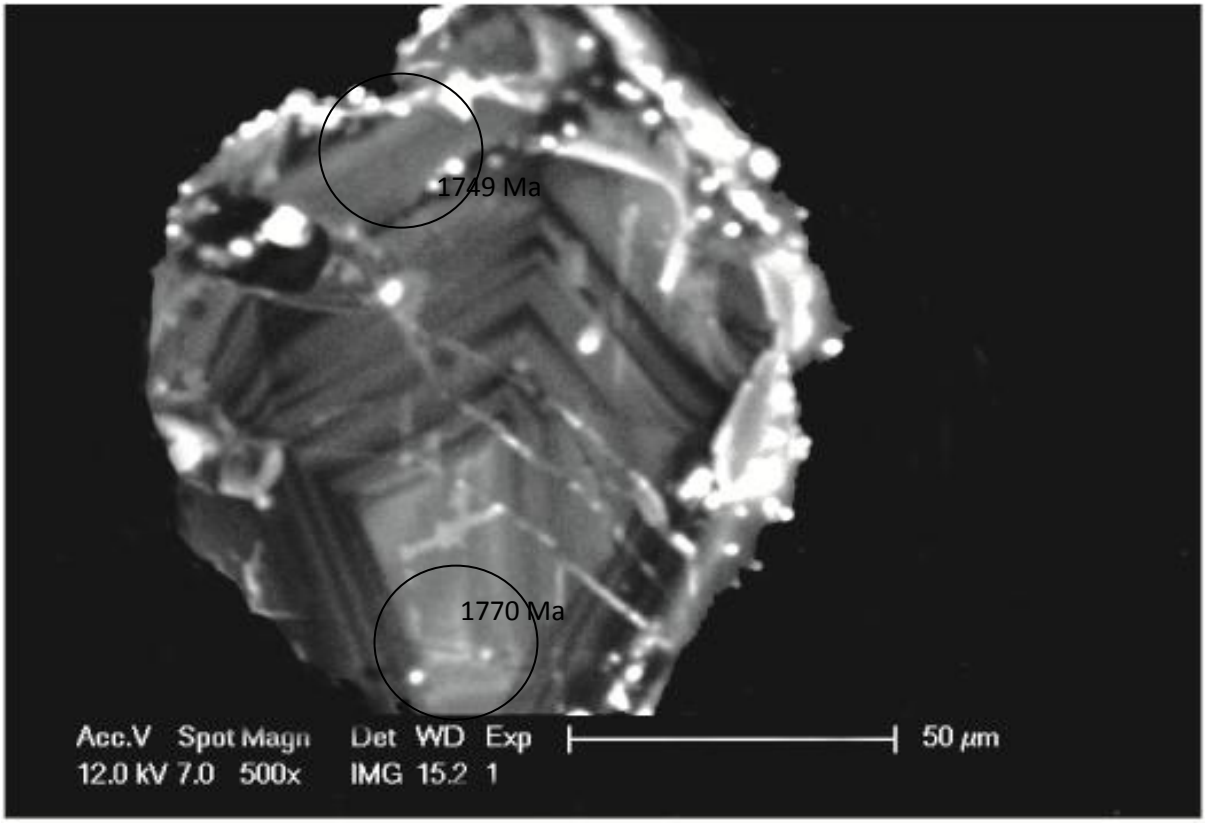
1749 Ma
1770 Ma
Acc.V Spot Magn Det WD Exp
12.0 kV 7.0 500x IMG 15.2 1
50 µm

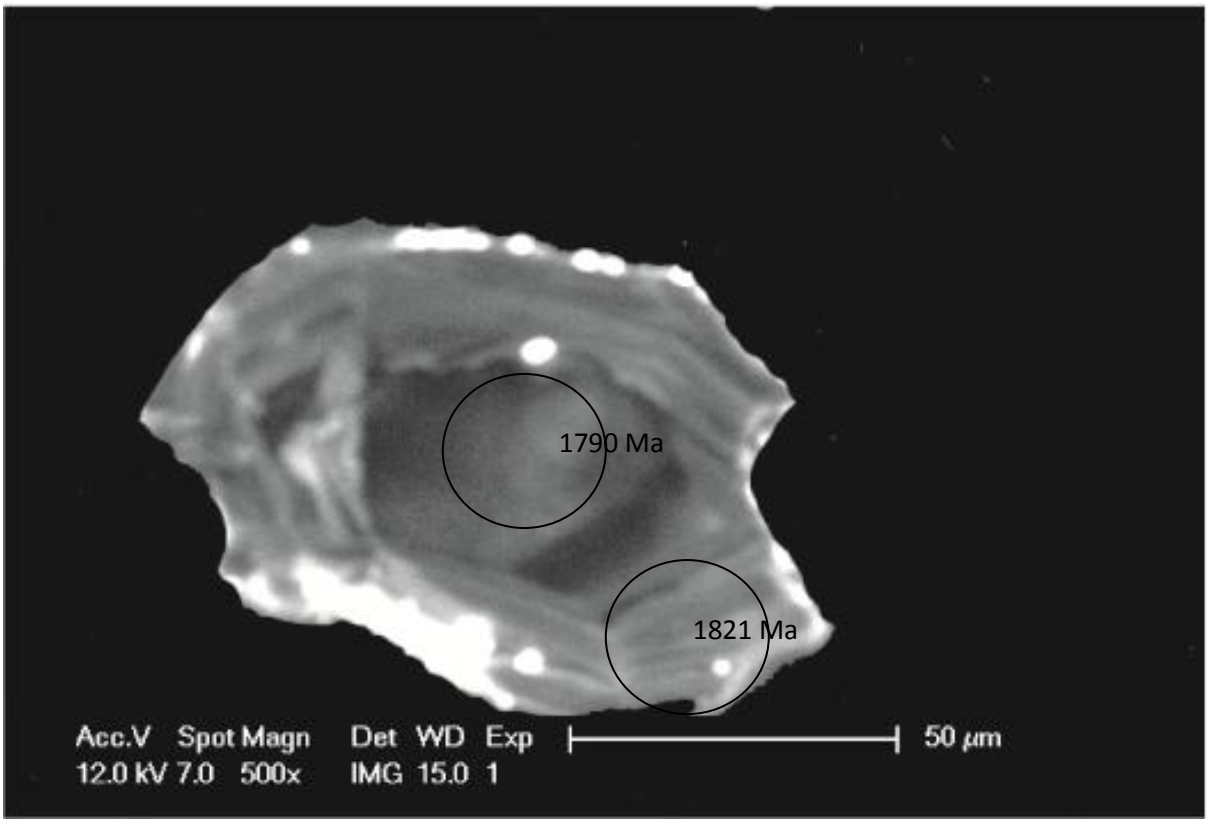
1790 Ma
1821 Ma
Acc.V Spot Magn Det WD Exp
12.0 kV 7.0 500x IMG 15.0 1
50 µm

Figure 12

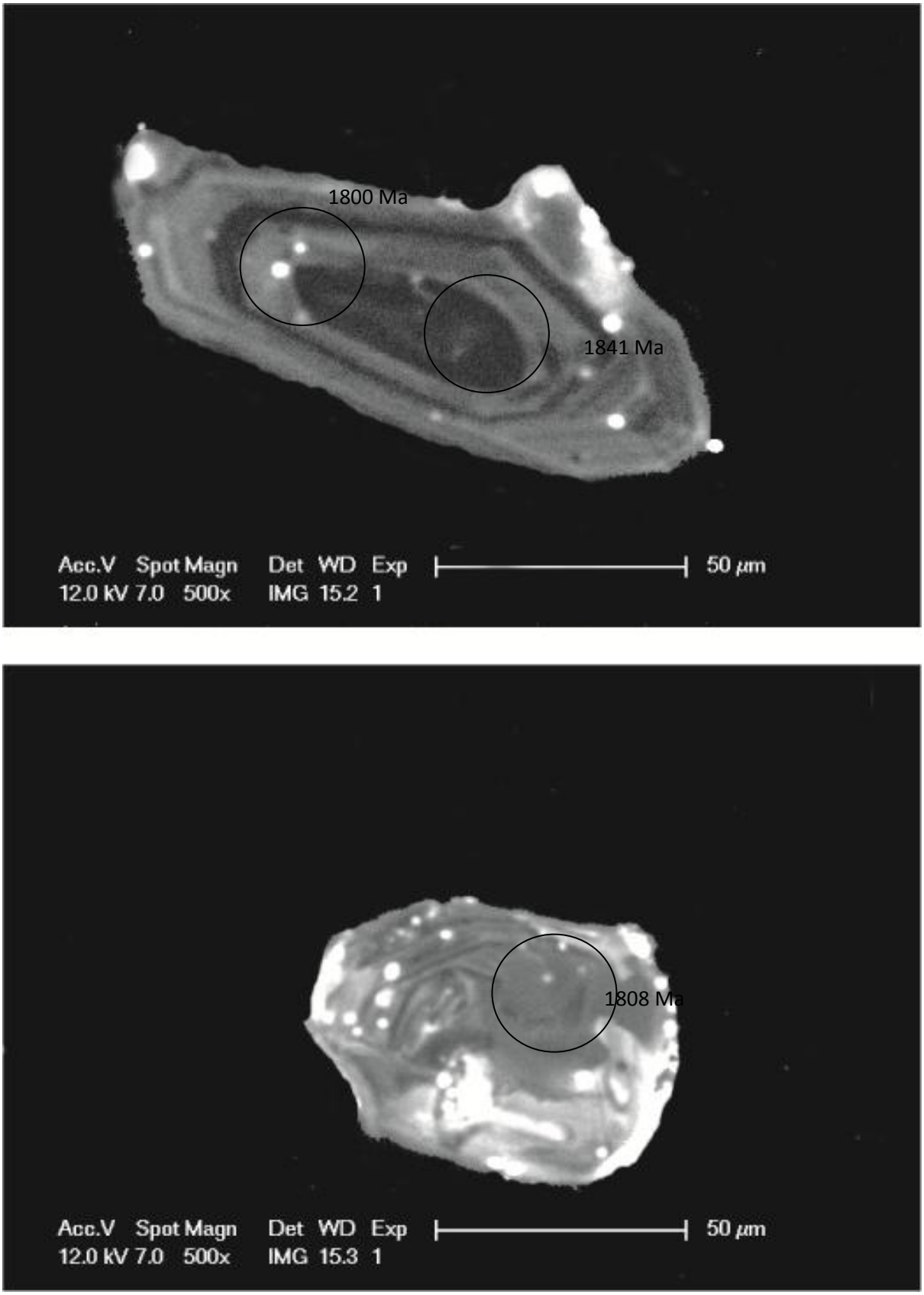
1800 Ma
1841 Ma
Acc.V Spot Magn Det WD Exp
12.0 kV 7.0 500x IMG 15.2 1
50 µm
1808 Ma
Acc.V Spot Magn Det WD Exp
12.0 kV 7.0 500x IMG 15.3 1
50 µm

Figure 13

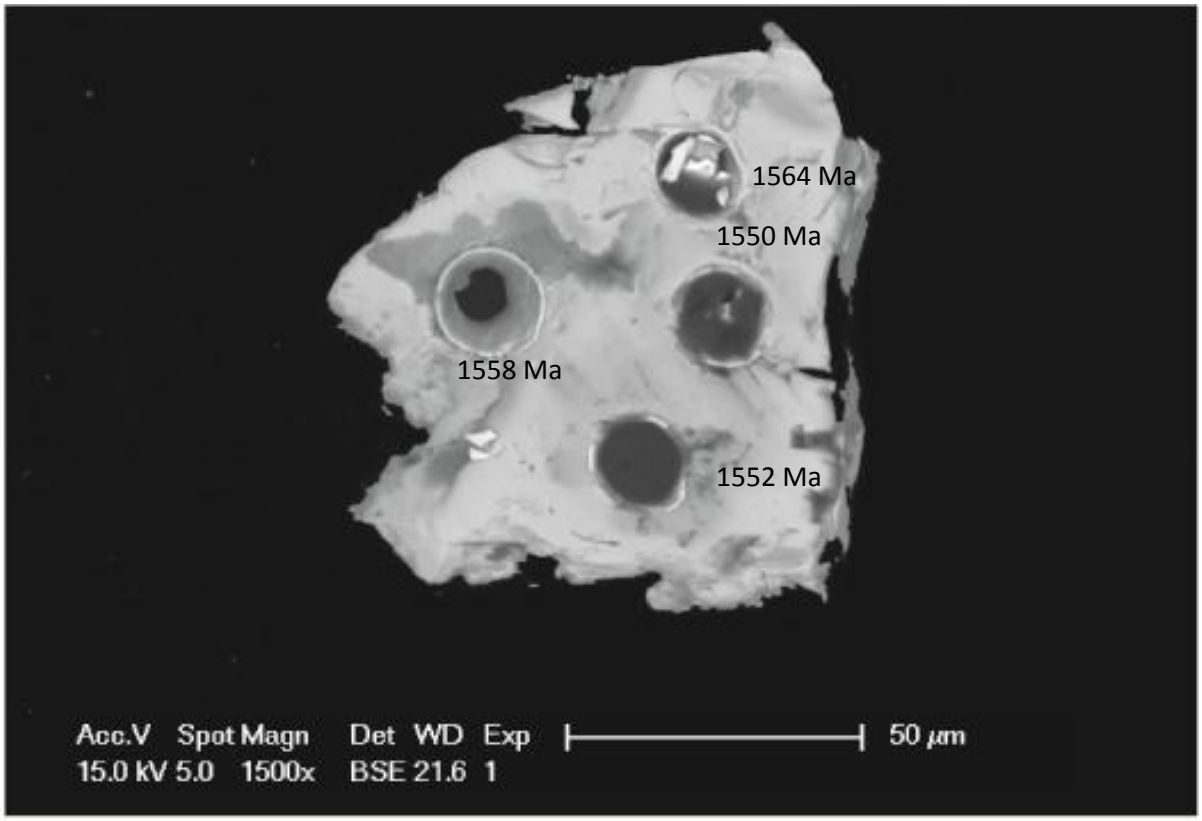
1564 Ma
1550 Ma
1558 Ma
1552 Ma
Acc.V Spot Magn Det WD Exp
15.0 kV 5.0 1500x BSE 21.6 1
50 µm

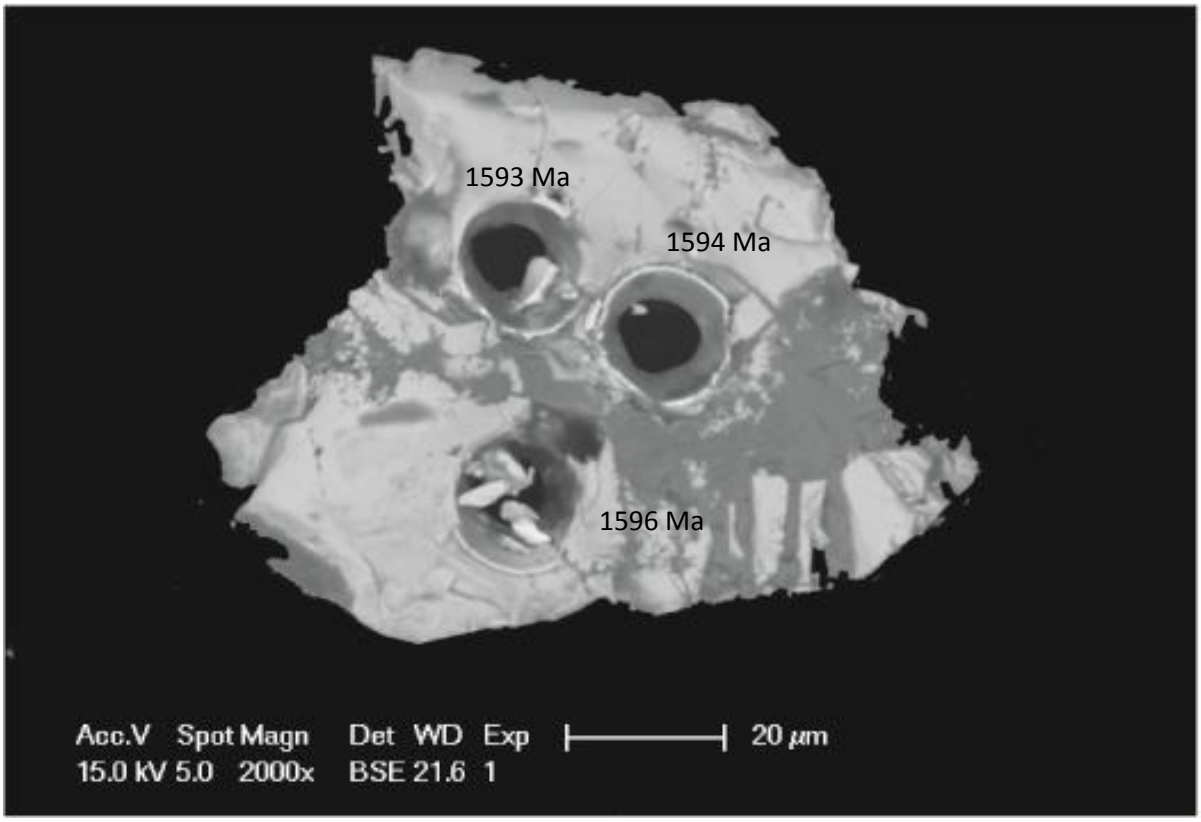
1593 Ma
1594 Ma
1596 Ma
Acc.V Spot Magn Det WD Exp
15.0 kV 5.0 2000x BSE 21.6 1
20 µm

Figure 14

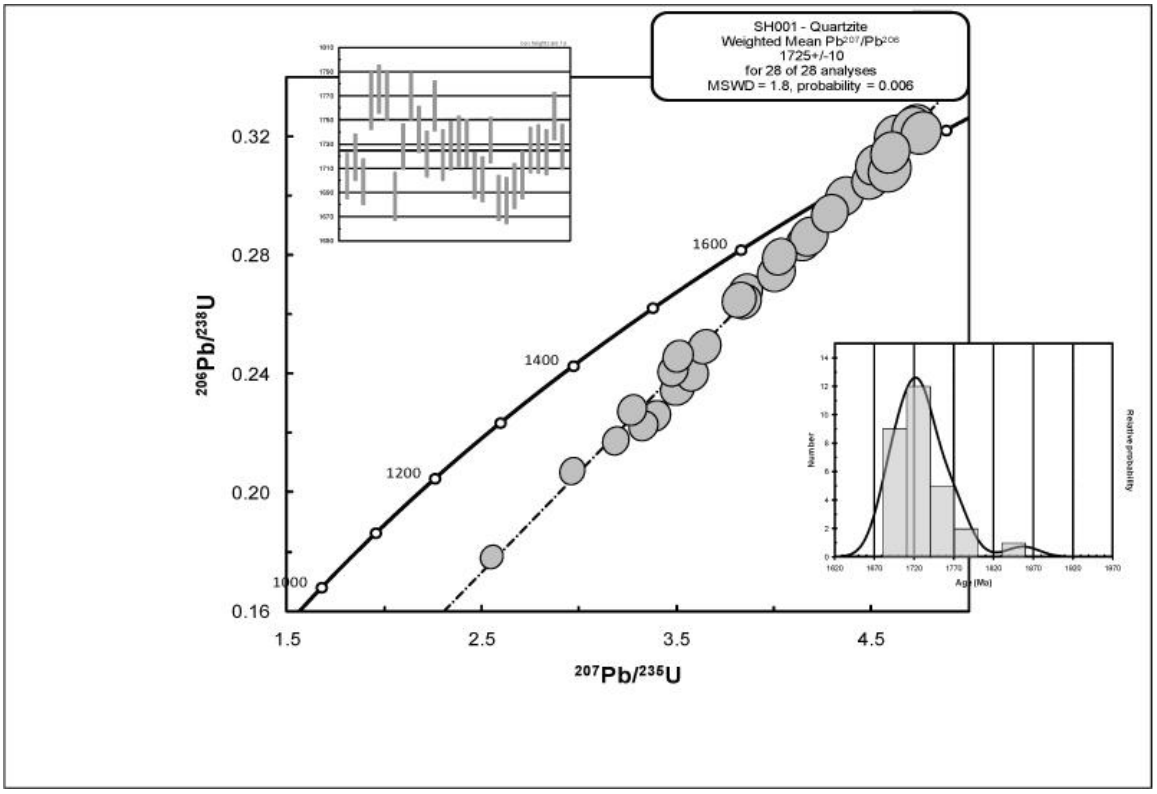
SH001 - Quartzite
Weighted Mean Pb207/Pb206
1725+/-10
for 28 of 28 analyses
MSWD = 1.8, probability = 0.006
0.32
0.28
0.24
0.20
0.16
206Pb/238U
1.5
2.5
3.5
4.5
207Pb/235U
1600
1400
1200
1000
Number
Relative probability
Age (Ma)

Figure 15

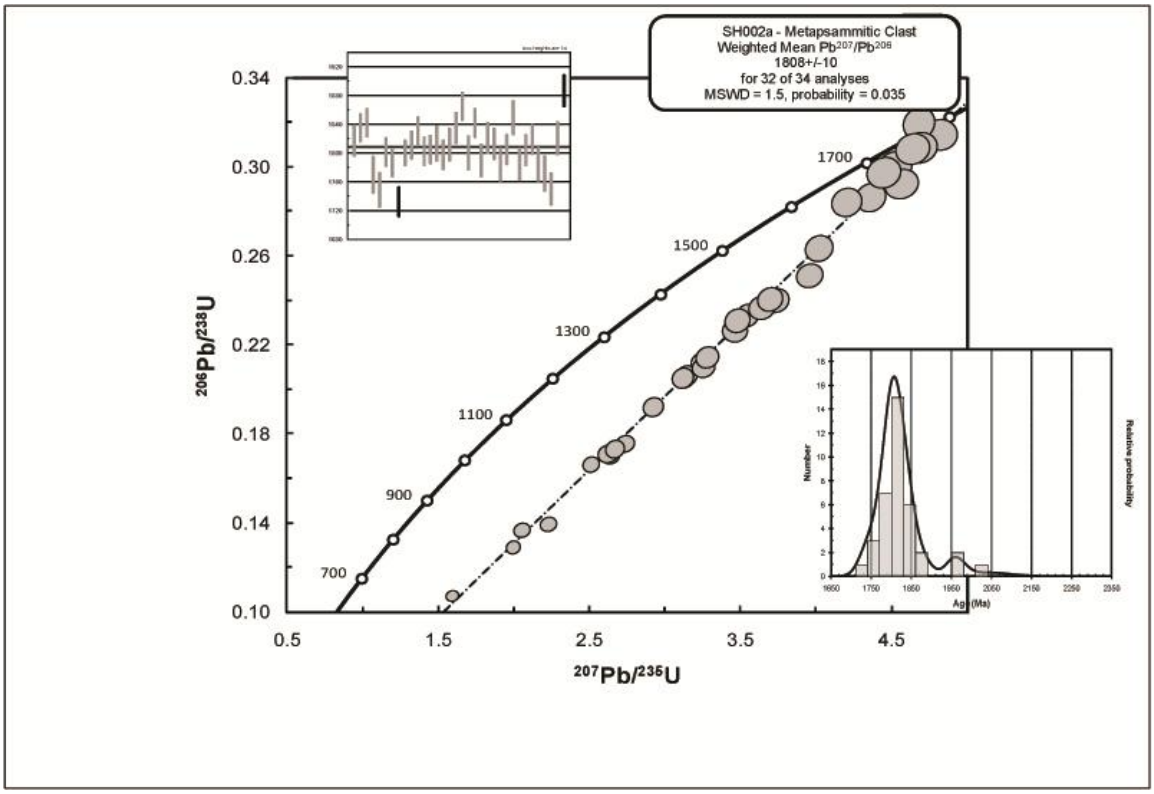
SH002a - Metapsammitic Clast
Weighted Mean Pb207/Pb206
1808+/-10
for 32 of 34 analyses
MSWD = 1.5, probability = 0.035
0.34
0.30
0.26
0.22
0.18
0.14
0.10
206Pb/238U
0.5
1.5
2.5
3.5
4.5
207Pb/235U
700
900
1100
1300
1500
1700
Number
Relative probability
Age (Ma)

Figure 16

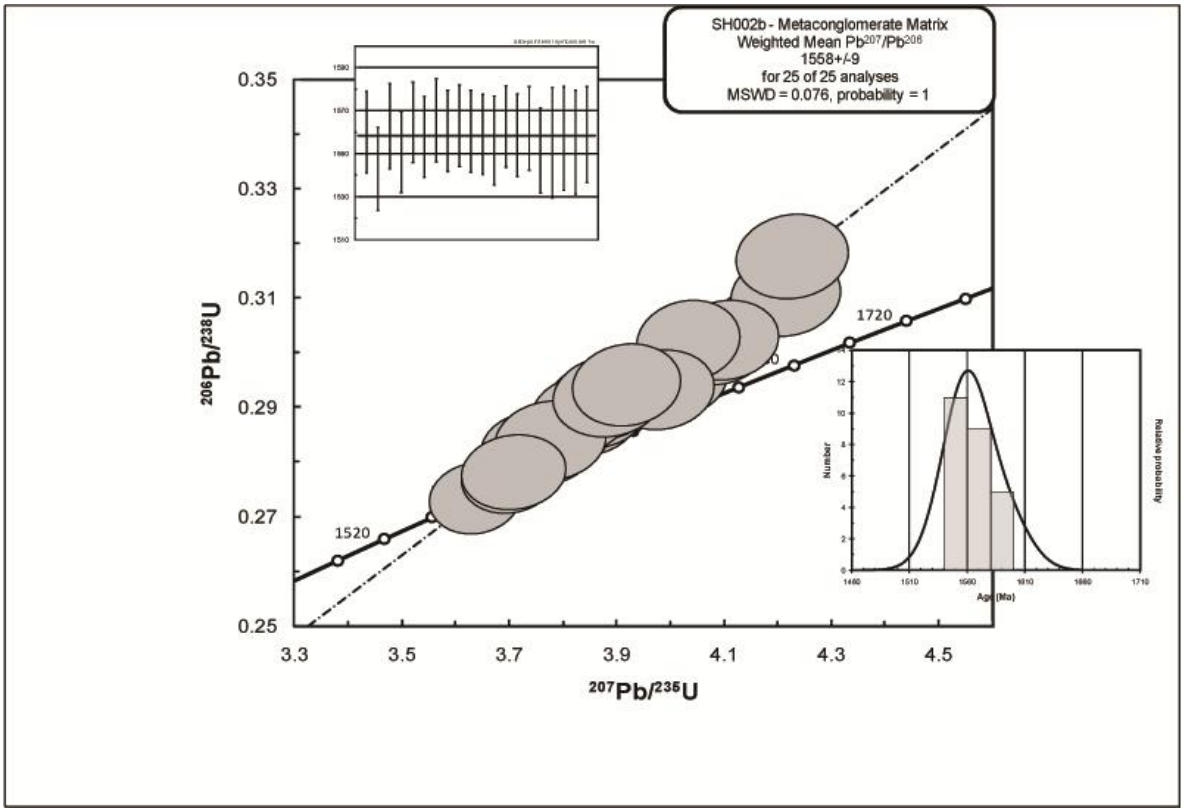
SH002b - Metaconglomerate Matrix
Weighted Mean Pb207/Pb206
1558+/-9
for 25 of 25 analyses
MSWD = 0.076, probability = 1
0.35
0.33
0.31
0.29
0.27
0.25
206Pb/238U
3.3
3.5
3.7
3.9
4.1
4.3
4.5
207Pb/235U
1520
1720
Number
Relative probability
Age (Ma)

Figure 17

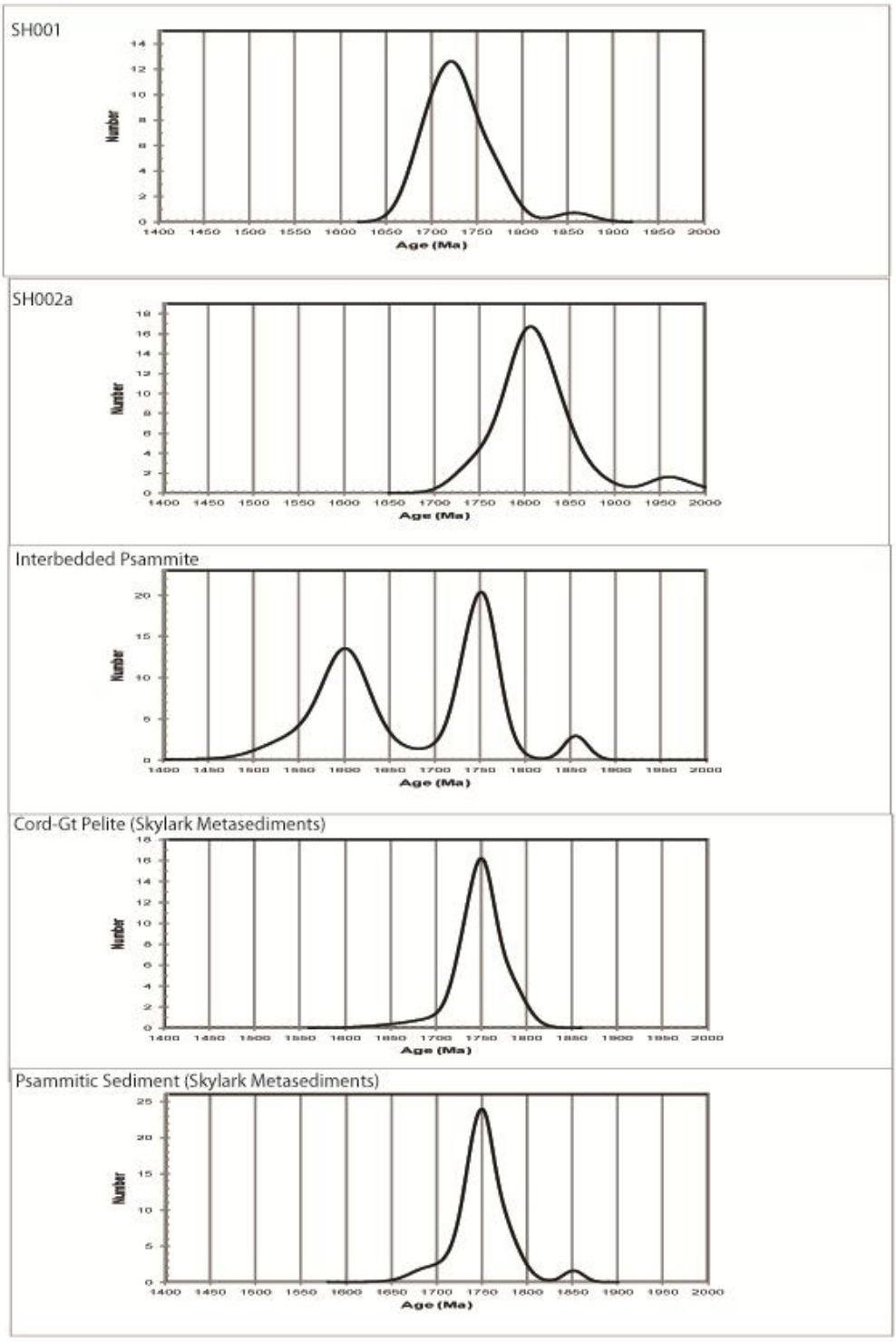
SH001
Number
Age (Ma)
SH002a
Number
Age (Ma)
Interbedded Psammite
Number
Age (Ma)
Cord-Gt Pelite (Skylark Metasediments)
Number
Age (Ma)
Psammitic Sediment (Skylark Metasediments)
Number
Age (Ma)

Figure 18

SH001

	Isotope Ratio							Age Estimates							
Spot	Pb207/Pb206	1σ	Pb207/U235	1σ	Pb206/U238	1σ	rho	Pb207/Pb206	1σ	Pb206/U238	1σ	Pb207/U235	1σ	Disc	Comment
1	0.1044	0.00109	4.60976	0.06539	0.32026	0.00457	0.1044	1703.8	19.03	1791	22.34	1751	11.84	-5.1179716	
2	0.10529	0.00111	4.35599	0.06215	0.3001	0.00429	0.10529	1719.3	19.22	1691.8	21.28	1704	11.78	1.5994882	
6	0.10824	0.00117	3.32269	0.04961	0.22268	0.00332	0.10824	1769.9	19.66	1296	17.5	1486.4	11.65	26.775524	
9	0.11355	0.00131	4.79454	0.06899	0.30626	0.00427	0.11355	1857	20.65	1722.3	21.05	1783.9	12.09	7.2536349	
10	0.10579	0.00108	4.15075	0.05908	0.2846	0.0041	0.10579	1728.1	18.63	1614.5	20.59	1664.4	11.65	6.5736937	
15	0.10539	0.00121	3.84249	0.05738	0.26451	0.00383	0.10539	1721.1	20.87	1512.9	19.54	1601.7	12.03	12.096915	
16	0.10583	0.00117	4.17695	0.06425	0.28633	0.00435	0.10583	1728.8	20.14	1623.2	21.81	1669.5	12.6	6.1082832	
18	0.10597	0.00113	3.64063	0.05557	0.2492	0.00379	0.10597	1731.3	19.38	1434.4	19.55	1558.5	12.16	17.148963	
19	0.10443	0.00109	3.47705	0.05126	0.24151	0.00356	0.10443	1704.4	19.15	1394.6	18.51	1522	11.63	18.176484	
20	0.10426	0.00106	4.02179	0.05837	0.2798	0.00412	0.10426	1701.3	18.61	1590.4	20.74	1638.6	11.8	6.5185446	
26	0.10563	0.00109	4.2848	0.06195	0.29426	0.00431	0.10563	1725.2	18.77	1662.8	21.48	1690.4	11.9	3.6169719	
27	0.10567	0.00115	4.71865	0.06961	0.32391	0.00475	0.10567	1726	19.87	1808.8	23.12	1770.6	12.36	-4.797219	

SH002b

	isotopic ratios							age estimates							
Spot	Pb207/Pb206	1σ	Pb207/U235	1σ	Pb206/U238	1σ	rho	Pb207/Pb206	1σ	Pb206/U238	1σ	Pb207/U235	1σ	Disc	Comment
1	0.09663	0.00098	4.12698	0.06299	0.3099	0.00484	0.97727	1560.1	18.97	1740.2	23.81	1659.7	12.48	-11.544132	
3	0.09677	0.00103	3.87863	0.06075	0.29094	0.00459	0.09677	1562.8	19.88	1646.2	22.93	1609.2	12.64	-5.3365754	
4	0.09615	0.00097	3.85875	0.05906	0.29127	0.00458	0.09615	1550.8	18.83	1647.9	22.84	1605.1	12.34	-6.2612845	
9	0.0985	0.00109	4.21243	0.06753	0.31058	0.00497	0.0985	1596	20.56	1743.6	24.46	1676.4	13.15	-9.2481203	
10	0.09836	0.00104	4.08526	0.06457	0.30143	0.00482	0.09836	1593.2	19.68	1698.4	23.88	1651.4	12.89	-6.603063	
11	0.09839	0.00103	4.10171	0.06462	0.30239	0.00483	0.09839	1593.9	19.43	1703.2	23.92	1654.6	12.86	-6.8573938	
12	0.09666	0.00097	3.88077	0.06049	0.29124	0.00466	0.09666	1560.6	18.77	1647.7	23.25	1609.7	12.58	-5.5811867	
14	0.09665	0.00098	3.769	0.05858	0.28279	0.00449	0.09665	1560.5	18.93	1605.4	22.56	1586.2	12.47	-2.8772829	
17	0.09676	0.00098	4.03182	0.06311	0.30225	0.00487	0.09676	1562.6	18.92	1702.5	24.12	1640.6	12.73	-8.953027	
18	0.09656	0.00099	3.87821	0.06047	0.29121	0.00461	0.09656	1558.6	19.17	1647.6	23	1609.2	12.59	-5.7102528	
19	0.09671	0.00101	3.69869	0.05846	0.27736	0.00444	0.09671	1561.7	19.39	1578.1	22.41	1571.1	12.63	-1.0501377	
24	0.09639	0.00125	3.88219	0.06842	0.29211	0.00492	0.09639	1555.3	24.17	1652.1	24.56	1610	14.23	-6.2238796	

Table 1

	Isotope Ratio							Age Estimates						
Spot	Pb207/Pb206	1σ	Pb207/U235	1σ	Pb206/U238	1σ	rho	Pb207/Pb206	1σ	Pb206/U238	1σ	Pb207/U235	1σ	Disc.
1a	0.11108	0.0013	4.81878	0.0735	0.31466	0.0046	0.0230515	1817.1	21.5	1763.6	22.6	1788.2	12.8	2.9442518
2a	0.1122	0.0012	2.63275	0.0379	0.17022	0.00242	0.1122	1835.4	19.73	1013.3	13.3	1309.8	10.6	44.791326
3a	0.11263	0.0012	2.7302	0.0399	0.17584	0.00255	0.11263	1842.2	19.74	1044.2	14	1336.7	10.9	43.317772
4a	0.10823	0.0015	2.04699	0.0351	0.13715	0.00212	0.10823	1769.8	25.71	828.5	12	1131.3	11.7	53.186801
5a	0.107	0.0014	1.5876	0.0256	0.10758	0.00161	0.107	1748.9	23.84	658.7	9.37	965.4	10.1	62.336326
6a	0.11012	0.0012	3.11744	0.046	0.20532	0.003	0.11012	1801.4	20.01	1203.8	16.1	1437	11.3	33.174198
8a	0.1092	0.0012	2.50499	0.0361	0.16648	0.00242	0.1092	1786.1	19.25	992.7	13.4	1273.5	10.5	44.420805
9a	0.12097	0.0015	3.58537	0.0556	0.21493	0.00321	0.12097	1970.5	21.7	1255.1	17.1	1546.3	12.3	36.305506
10a	0.10604	0.0012	4.67387	0.0689	0.31976	0.00466	0.10604	1732.4	20.26	1788.6	22.7	1762.6	12.3	-3.2440545
11a	0.11007	0.0011	3.54071	0.0501	0.2334	0.0034	0.11007	1800.5	17.96	1352.3	17.8	1536.4	11.2	24.893085
12a	0.1107	0.0012	3.23837	0.0475	0.21224	0.00311	0.1107	1811	19.47	1240.7	16.5	1466.4	11.4	31.490889
15a	0.11189	0.0013	1.9913	0.03	0.12923	0.00192	0.11189	1830.4	20.46	783.4	11	1112.6	10.2	57.200612
1b	0.11075	0.0014	3.4546	0.0545	0.22641	0.00332	0.0320587	1811.7	22.87	1315.7	17.5	1516.9	12.4	27.377601
2b	0.11217	0.0014	3.2491	0.0498	0.21015	0.00304	0.11217	1834.9	21.77	1229.6	16.2	1469	11.9	32.988174
3b	0.11407	0.0012	3.95088	0.0568	0.25125	0.00357	0.11407	1865.3	19.41	1444.9	18.4	1624.2	11.6	22.53793
4b	0.11006	0.0014	4.68101	0.0752	0.30859	0.00455	0.11006	1800.3	23.65	1733.8	22.4	1763.9	13.4	3.6938288
5b	0.1126	0.0013	3.72887	0.0553	0.24024	0.00347	0.1126	1841.7	20.24	1387.9	18	1577.6	11.9	24.640278
6b	0.10941	0.0014	4.51644	0.0715	0.29955	0.00447	0.10941	1789.6	22.56	1689.1	22.2	1734	13.2	5.6157801
7b	0.11132	0.0013	3.63524	0.0562	0.23688	0.00349	0.11132	1821.1	21.48	1370.5	18.2	1557.3	12.3	24.743287
8b	0.11081	0.0013	3.27642	0.0498	0.21449	0.0031	0.11081	1812.8	21.45	1252.7	16.4	1475.5	11.8	30.896955
9b	0.10907	0.0014	4.51742	0.0719	0.30043	0.00441	0.10907	1784	23.22	1693.4	21.8	1734.2	13.2	5.0784753
10b	0.11034	0.0013	4.01134	0.0608	0.26369	0.00384	0.11034	1805	20.95	1508.7	19.6	1636.5	12.3	16.415512
11b	0.11306	0.0015	4.55908	0.0733	0.29258	0.00435	0.11306	1849.1	23.48	1654.4	21.7	1741.8	13.4	10.529447
14b	0.11029	0.0013	4.3567	0.0666	0.28658	0.00422	0.11029	1804.1	21.49	1624.4	21.2	1704.2	12.6	9.9606452

Table 2

Appendix A

	Isotope Ratio							Age Estimates							
Spot	Pb207/Pb206	1σ	Pb207/U235	1σ	Pb206/U238	1σ	rho	Pb207/Pb206	1σ	Pb206/U238	1σ	Pb207/U235	1σ	Disc	Comment
1	0.1044	0.00109	4.60976	0.06539	0.32026	0.00457	0.1044	1703.8	19.03	1791	22.34	1751	11.84	-5.1179716	
2	0.10529	0.00111	4.35599	0.06215	0.3001	0.00429	0.10529	1719.3	19.22	1691.8	21.28	1704	11.78	1.5994882	
3	0.10413	0.00107	3.84855	0.05575	0.26808	0.00393	0.10413	1699	18.82	1531.1	19.97	1603	11.68	9.8822837	
4	0.108	0.0014	3.49753	0.0578	0.23509	0.00365	0.108	1765.9	23.51	1361.1	19.07	1526.7	13.05	22.923155	
5	0.10858	0.0012	3.38374	0.05155	0.22608	0.00343	0.10858	1775.6	19.98	1313.9	18.05	1500.6	11.94	26.002478	
6	0.10824	0.00117	3.32269	0.04961	0.22268	0.00332	0.10824	1769.9	19.66	1296	17.5	1486.4	11.65	26.775524	
7	0.13484	0.00174	5.40546	0.0886	0.29083	0.00453	0.13484	2161.9	22.33	1645.7	22.6	1885.7	14.04	23.877145	Monazite
8	0.10345	0.00112	2.54448	0.03837	0.17844	0.00268	0.10345	1686.8	19.87	1058.4	14.65	1284.9	10.99	37.253972	
9	0.11355	0.00131	4.79454	0.06899	0.30626	0.00427	0.11355	1857	20.65	1722.3	21.05	1783.9	12.09	7.2536349	
10	0.10579	0.00108	4.15075	0.05908	0.2846	0.0041	0.10579	1728.1	18.63	1614.5	20.59	1664.4	11.65	6.5736937	
11	0.10825	0.00114	3.57634	0.05204	0.23967	0.00349	0.10825	1770	19.19	1385	18.15	1544.3	11.55	21.751412	
12	0.10662	0.0011	4.49122	0.06451	0.30559	0.00443	0.10662	1742.4	18.81	1719	21.85	1729.4	11.93	1.3429752	
13	0.10544	0.00108	4.51303	0.06487	0.31049	0.00451	0.10544	1722	18.78	1743.1	22.17	1733.4	11.95	-1.2253194	
14	0.10775	0.00123	4.58693	0.07216	0.30882	0.00474	0.10775	1761.8	20.74	1734.9	23.37	1746.9	13.11	1.5268475	
15	0.10539	0.00121	3.84249	0.05738	0.26451	0.00383	0.10539	1721.1	20.87	1512.9	19.54	1601.7	12.03	12.096915	
16	0.10583	0.00117	4.17695	0.06425	0.28633	0.00435	0.10583	1728.8	20.14	1623.2	21.81	1669.5	12.6	6.1082832	
17	0.10605	0.0012	4.00716	0.06253	0.27411	0.00421	0.10605	1732.6	20.56	1561.6	21.29	1635.6	12.68	9.8695602	
18	0.10597	0.00113	3.64063	0.05557	0.2492	0.00379	0.10597	1731.3	19.38	1434.4	19.55	1558.5	12.16	17.148963	
19	0.10443	0.00109	3.47705	0.05126	0.24151	0.00356	0.10443	1704.4	19.15	1394.6	18.51	1522	11.63	18.176484	
20	0.10426	0.00106	4.02179	0.05837	0.2798	0.00412	0.10426	1701.3	18.61	1590.4	20.74	1638.6	11.8	6.5185446	
21	0.1061	0.00109	3.18359	0.04589	0.21767	0.00317	0.1061	1733.5	18.71	1269.6	16.78	1453.2	11.14	26.760888	
22	0.10337	0.00106	2.95735	0.0423	0.20752	0.003	0.10337	1685.6	18.72	1215.6	16.04	1396.7	10.85	27.883246	
23	0.10326	0.00108	3.50293	0.05135	0.24607	0.00362	0.10326	1683.5	19.14	1418.2	18.75	1527.9	11.58	15.758836	
24	0.10393	0.00106	3.26663	0.04766	0.22799	0.00336	0.10393	1695.5	18.68	1324	17.66	1473.1	11.34	21.910941	
25	0.10445	0.00112	3.81668	0.05624	0.26505	0.00389	0.10445	1704.7	19.69	1515.6	19.83	1596.3	11.86	11.092861	
26	0.10563	0.00109	4.2848	0.06195	0.29426	0.00431	0.10563	1725.2	18.77	1662.8	21.48	1690.4	11.9	3.6169719	
27	0.10567	0.00115	4.71865	0.06961	0.32391	0.00475	0.10567	1726	19.87	1808.8	23.12	1770.6	12.36	-4.797219	
28	0.10552	0.00108	4.70217	0.06719	0.32322	0.00469	0.10552	1723.5	18.62	1805.4	22.87	1767.6	11.97	-4.7519582	
29	0.10725	0.00116	4.75106	0.06959	0.3213	0.00469	0.10725	1753.3	19.57	1796.1	22.86	1776.3	12.29	-2.441111	
30	0.10578	0.00107	4.59233	0.0653	0.31489	0.00456	0.10578	1727.9	18.53	1764.7	22.34	1747.9	11.86	-2.1297529	

Table 1

	Isotope Ratio							Age Estimates							
Spot	Pb207/Pb206	1σ	Pb207/U235	1σ	Pb206/U238	1σ	rho	Pb207/Pb206	1σ	Pb206/U238	1σ	Pb207/U235	1σ	Disc.	
1	0.11108	0.0013	4.81878	0.0735	0.31466	0.0046	0.0230515	1817.1	21.5	1763.6	22.6	1788.2	12.8	2.9442518	
2	0.1122	0.0012	2.63275	0.0379	0.17022	0.00242	0.1122	1835.4	19.73	1013.3	13.3	1309.8	10.6	44.791326	
3	0.11263	0.0012	2.7302	0.0399	0.17584	0.00255	0.11263	1842.2	19.74	1044.2	14	1336.7	10.9	43.317772	
4	0.10823	0.0015	2.04699	0.0351	0.13715	0.00212	0.10823	1769.8	25.71	828.5	12	1131.3	11.7	53.186801	
5	0.107	0.0014	1.5876	0.0256	0.10758	0.00161	0.107	1748.9	23.84	658.7	9.37	965.4	10.1	62.336326	
6	0.11012	0.0012	3.11744	0.046	0.20532	0.003	0.11012	1801.4	20.01	1203.8	16.1	1437	11.3	33.174198	
~~7~~	~~0.73642~~	~~0.018~~	~~244.18098~~	~~7.4215~~	~~2.40551~~	~~0.0777~~	~~0.73642~~	~~4803.5~~	~~34.54~~	~~7899.4~~	~~147~~	~~5586.6~~	~~30.7~~	-64.450921	Monazite
8	0.1092	0.0012	2.50499	0.0361	0.16648	0.00242	0.1092	1786.1	19.25	992.7	13.4	1273.5	10.5	44.420805	
9	0.12097	0.0015	3.58537	0.0556	0.21493	0.00321	0.12097	1970.5	21.7	1255.1	17.1	1546.3	12.3	36.305506	
10	0.10604	0.0012	4.67387	0.0689	0.31976	0.00466	0.10604	1732.4	20.26	1788.6	22.7	1762.6	12.3	-3.2440545	
11	0.11007	0.0011	3.54071	0.0501	0.2334	0.0034	0.11007	1800.5	17.96	1352.3	17.8	1536.4	11.2	24.893085	
12	0.1107	0.0012	3.23837	0.0475	0.21224	0.00311	0.1107	1811	19.47	1240.7	16.5	1466.4	11.4	31.490889	
13	0.11968	0.0014	3.27252	0.0488	0.19842	0.00292	0.11968	1951.4	19.95	1166.8	15.7	1474.5	11.6	40.207031	
~~14~~	~~0.14946~~	~~0.0015~~	~~3.87419~~	~~0.0551~~	~~0.18805~~	~~0.00272~~	~~0.14946~~	~~2339.8~~	~~17.21~~	~~1110.8~~	~~14.8~~	~~1608.3~~	~~11.5~~	~~52.525857~~	Fractured
15	0.11189	0.0013	1.9913	0.03	0.12923	0.00192	0.11189	1830.4	20.46	783.4	11	1112.6	10.2	57.200612	
16	0.1102	0.0012	2.91804	0.0433	0.1921	0.00281	0.1102	1802.7	20.04	1132.8	15.2	1386.6	11.2	37.160925	
17	0.11033	0.0012	3.13551	0.0458	0.20614	0.00299	0.11033	1804.9	19.54	1208.2	16	1441.4	11.3	33.060003	
18	0.11086	0.0015	2.61931	0.0431	0.17137	0.00263	0.11086	1813.6	24.49	1019.7	14.5	1306.1	12.1	43.774813	
19	0.1099	0.0012	3.10925	0.0464	0.20527	0.00306	0.1099	1797.7	20.33	1203.6	16.4	1435	11.5	33.047783	
1	0.11075	0.0014	3.4546	0.0545	0.22641	0.00332	0.0320587	1811.7	22.87	1315.7	17.5	1516.9	12.4	27.377601	
2	0.11217	0.0014	3.2491	0.0498	0.21015	0.00304	0.11217	1834.9	21.77	1229.6	16.2	1469	11.9	32.988174	
3	0.11407	0.0012	3.95088	0.0568	0.25125	0.00357	0.11407	1865.3	19.41	1444.9	18.4	1624.2	11.6	22.53793	
4	0.11006	0.0014	4.68101	0.0752	0.30859	0.00455	0.11006	1800.3	23.65	1733.8	22.4	1763.9	13.4	3.6938288	
5	0.1126	0.0013	3.72887	0.0553	0.24024	0.00347	0.1126	1841.7	20.24	1387.9	18	1577.6	11.9	24.640278	
6	0.10941	0.0014	4.51644	0.0715	0.29955	0.00447	0.10941	1789.6	22.56	1689.1	22.2	1734	13.2	5.6157801	
7	0.11132	0.0013	3.63524	0.0562	0.23688	0.00349	0.11132	1821.1	21.48	1370.5	18.2	1557.3	12.3	24.743287	
8	0.11081	0.0013	3.27642	0.0498	0.21449	0.0031	0.11081	1812.8	21.45	1252.7	16.4	1475.5	11.8	30.896955	
9	0.10907	0.0014	4.51742	0.0719	0.30043	0.00441	0.10907	1784	23.22	1693.4	21.8	1734.2	13.2	5.0784753	
10	0.11034	0.0013	4.01134	0.0608	0.26369	0.00384	0.11034	1805	20.95	1508.7	19.6	1636.5	12.3	16.415512	
11	0.11306	0.0015	4.55908	0.0733	0.29258	0.00435	0.11306	1849.1	23.48	1654.4	21.7	1741.8	13.4	10.529447	
12	0.10911	0.0014	4.63406	0.0722	0.30813	0.00454	0.10911	1784.5	22.51	1731.5	22.4	1755.4	13	2.9700196	
~~13~~	~~0.13137~~	~~0.0016~~	~~5.87961~~	~~0.091~~	~~0.32473~~	~~0.00482~~	~~0.13137~~	~~2116.4~~	~~21.32~~	~~1812.8~~	~~23.4~~	~~1958.2~~	~~13.4~~	~~14.345114~~	Monazite

14	0.11029	0.0013	4.3567	0.0666	0.28658	0.00422	0.11029	1804.1	21.49	1624.4	21.2	1704.2	12.6	9.9606452								
15	0.11119	0.0013	3.68695	0.0549	0.24051	0.00351	0.11119	1819	20.61	1389.4	18.2	1568.5	11.9	23.617372								
16	0.10911	0.0014	3.47194	0.0553	0.23094	0.00346	0.10911	1784.5	23.4	1339.4	18.1	1520.9	12.6	24.942561								
17	0.10832	0.0015	4.44295	0.0726	0.29766	0.00449	0.10832	1771.4	24.42	1679.7	22.3	1720.4	13.5	5.1766964								
18	0.10706	0.0013	4.19645	0.0655	0.2844	0.00424	0.10706	1749.9	22.38	1613.5	21.3	1673.3	12.8	7.7947311								
19	0.1113	0.0014	2.66174	0.0424	0.17356	0.00262	0.1113	1820.7	23.02	1031.7	14.4	1317.9	11.8	43.334981								
20	0.11544	0.0014	2.22066	0.0345	0.13957	0.00208	0.11544	1886.8	22.21	842.2	11.8	1187.6	10.9	55.363579								
21	0.12568	0.0041	2.75669	0.087	0.15912	0.00327	0.12568	2038.4	56.58	951.9	18.2	1343.9	23.5	53.301609								

Table 2

	isotopic ratios							age estimates							
Spot	Pb207/Pb206	1σ	Pb207/U235	1σ	Pb206/U238	1σ	rho	Pb207/Pb206	1σ	Pb206/U238	1σ	Pb207/U235	1σ	Disc	Comment
1	0.09663	0.00098	4.12698	0.06299	0.3099	0.00484	0.977272	1560.1	18.97	1740.2	23.8	1659.7	12.48	-11.544132	
2	0.09576	0.00098	3.73092	0.05655	0.28255	0.00438	0.09576	1543	19.2	1604.2	22	1578	12.14	-3.9662994	
3	0.09677	0.00103	3.87863	0.06075	0.29094	0.00459	0.09677	1562.8	19.88	1646.2	22.9	1609.2	12.64	-5.3365754	
4	0.09615	0.00097	3.85875	0.05906	0.29127	0.00458	0.09615	1550.8	18.83	1647.9	22.8	1605.1	12.34	-6.2612845	
5	0.09687	0.00097	3.88855	0.05895	0.2912	0.00455	0.09687	1564.6	18.62	1647.5	22.7	1611.3	12.24	-5.2984788	
6	0.09652	0.00097	3.63422	0.05592	0.27342	0.00432	0.09652	1557.9	18.75	1558.1	21.9	1557.1	12.25	-0.0128378	
7	0.09691	0.00101	3.84777	0.05996	0.28824	0.00457	0.09691	1565.5	19.37	1632.7	22.9	1602.8	12.56	-4.2925583	
8	0.09855	0.00107	4.00686	0.06364	0.29532	0.00471	0.09855	1596.8	20.14	1668.1	23.5	1635.6	12.91	-4.4651804	
9	0.0985	0.00109	4.21243	0.06753	0.31058	0.00497	0.0985	1596	20.56	1743.6	24.5	1676.4	13.15	-9.2481203	
10	0.09836	0.00104	4.08526	0.06457	0.30143	0.00482	0.09836	1593.2	19.68	1698.4	23.9	1651.4	12.89	-6.603063	
11	0.09839	0.00103	4.10171	0.06462	0.30239	0.00483	0.09839	1593.9	19.43	1703.2	23.9	1654.6	12.86	-6.8573938	
12	0.09666	0.00097	3.88077	0.06049	0.29124	0.00466	0.09666	1560.6	18.77	1647.7	23.3	1609.7	12.58	-5.5811867	
13	0.09678	0.00098	3.86471	0.06013	0.28961	0.00462	0.09678	1563	18.85	1639.6	23.1	1606.3	12.55	-4.9008317	
14	0.09665	0.00098	3.769	0.05858	0.28279	0.00449	0.09665	1560.5	18.93	1605.4	22.6	1586.2	12.47	-2.8772829	
15	0.09657	0.00096	3.80057	0.05807	0.28535	0.00446	0.09657	1558.9	18.61	1618.2	22.4	1592.9	12.28	-3.8039643	
16	0.09643	0.00107	4.22476	0.06844	0.31778	0.00513	0.09643	1556.1	20.68	1778.9	25.1	1678.8	13.3	-14.317846	
17	0.09676	0.00098	4.03182	0.06311	0.30225	0.00487	0.09676	1562.6	18.92	1702.5	24.1	1640.6	12.73	-8.953027	
18	0.09656	0.00099	3.87821	0.06047	0.29121	0.00461	0.09656	1558.6	19.17	1647.6	23	1609.2	12.59	-5.7102528	
19	0.09671	0.00101	3.69869	0.05846	0.27736	0.00444	0.09671	1561.7	19.39	1578.1	22.4	1571.1	12.63	-1.0501377	
20	0.09619	0.00101	3.83014	0.06092	0.2888	0.00465	0.09619	1551.5	19.64	1635.5	23.3	1599.1	12.81	-5.4141154	
21	0.09638	0.00133	3.77452	0.06835	0.28401	0.00477	0.09638	1555.1	25.62	1611.5	24	1587.3	14.54	-3.6267764	
22	0.09838	0.00114	3.98059	0.06625	0.29338	0.00483	0.09838	1593.7	21.51	1658.4	24.1	1630.2	13.51	-4.0597352	
23	0.09648	0.00124	3.70596	0.06386	0.27824	0.0046	0.09648	1557.1	23.95	1582.5	23.2	1572.7	13.78	-1.6312376	
24	0.09639	0.00125	3.88219	0.06842	0.29211	0.00492	0.09639	1555.3	24.17	1652.1	24.6	1610	14.23	-6.2238796	
~~25~~	~~0.25113~~	~~0.01168~~	~~11.72444~~	~~0.49585~~	~~0.33878~~	~~0.01112~~	~~0.25113~~	~~3191.9~~	~~71.71~~	~~1880.8~~	~~53.6~~	~~2582.7~~	~~39.57~~	~~41.075848~~	Large Disc.
26	0.09657	0.00115	3.91601	0.06686	0.29421	0.00496	0.09657	1558.9	22.25	1662.5	24.7	1617	13.81	-6.6457117	

Table 3